

Spring 2011

Guidance, Navigation and Control of a Fly-By-Wire Transport Category Airship Designed for Hover Cargo Delivery

Harshad H. Lalan

Embry-Riddle Aeronautical University - Daytona Beach

Follow this and additional works at: <https://commons.erau.edu/db-theses>



Part of the [Aviation Commons](#)

Scholarly Commons Citation

Lalan, Harshad H., "Guidance, Navigation and Control of a Fly-By-Wire Transport Category Airship Designed for Hover Cargo Delivery" (2011). *Theses - Daytona Beach*. 110.
<https://commons.erau.edu/db-theses/110>

This thesis is brought to you for free and open access by Embry-Riddle Aeronautical University – Daytona Beach at ERAU Scholarly Commons. It has been accepted for inclusion in the Theses - Daytona Beach collection by an authorized administrator of ERAU Scholarly Commons. For more information, please contact commons@erau.edu.

**GUIDANCE, NAVIGATION AND CONTROL OF A FLY-BY-WIRE
TRANSPORT CATEGORY AIRSHIP DESIGNED FOR HOVER
CARGO DELIVERY**

by

Harshad H. Lalan

**A Thesis Submitted to the
Graduate Studies Office
In Partial Fulfillment of the Requirements for the
Degree of Master of Science in Aerospace Engineering**

**Embry-Riddle Aeronautical University
Daytona Beach, Florida
Spring 2011**

UMI Number: EP33521

All rights reserved

INFORMATION TO ALL USERS

The quality of this reproduction is dependent on the quality of the copy submitted.

In the unlikely event that the author did not send a complete manuscript and there are missing pages, these will be noted. Also, if material had to be removed, a note will indicate the deletion.



UMI EP33521

Copyright 2012 by ProQuest LLC.

All rights reserved. This edition of the work is protected against unauthorized copying under Title 17, United States Code.



ProQuest LLC.
789 East Eisenhower Parkway
P.O. Box 1346
Ann Arbor, MI 48106 - 1346

Copyright by Harshad H. Lalan 2011

All Rights Reserved

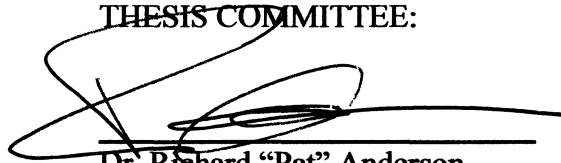
GUIDANCE, NAVIGATION AND CONTROL OF A FLY-BY-WIRE TRANSPORT
CATEGORY AIRSHIP DESIGNED FOR HOVER CARGO DELIVERY

by

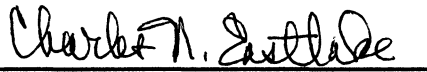
Harshad H. Lalan

This thesis was prepared under the direction of the candidate's thesis committee chairman, Dr. Richard "Pat" Anderson, Department of Aerospace Engineering, and has been approved by the members of his thesis committee. It was submitted to the Department of Aerospace Engineering and was accepted in partial fulfillment of the requirements for the degree of Master of Science in Aerospace Engineering.

THESIS COMMITTEE:



Dr. Richard "Pat" Anderson
Chairman



Professor Charles Eastlake
Member



Dr. Charles Reinholtz
Member



Coordinator, MSAE Program

5/12/11

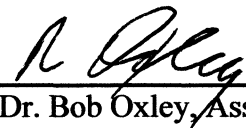
Date



Department Chair, Aerospace Engineering

5/12/11

Date



Dr. Bob Oxley, Associate VP for Academics

5/12/11

Date

ACKNOWLEDGEMENTS

This thesis arose in part out of the last two years of research that has been done on Airship Control Systems at Eagle Flight Research Center. I have worked with a great number of people, whose contributions in assorted ways to the research and making of the thesis deserve special mention. It is a pleasure to convey my gratitude to them all in my humble acknowledgment.

First, I would like to thank Dr. Anderson for his advice, supervision and crucial contribution which have made him a backbone of this thesis. I owe my deepest gratitude to Dr. Reinholtz for all of his advice and knowledge, which have played a major role in completing this thesis. I would also like to thank Prof. Eastlake for guiding me throughout the research process.

I would like to thank all my friends and coworkers who have helped and supported my work. I thank all the volunteers who helped to build the airship. I would also like to show my gratitude to Jason Lee for all his help and for working with me from the very beginning to the end. I would like to acknowledge Alex Perez, Enrique Bosche, Geoffrey London, and Evan Sales for their major contribution to this project. I also want to especially thank Ankit Nanda, Kashif Ali, and Prateek Jain for being there, even after hours. Lori—thanks for cheering me up when things didn't seem to go well. Also special thanks to Jeanette Barott for helping in editing and formatting this thesis. I am forever indebted to Shirley Koelker, who provided me the motivation and support to complete this thesis, and always provided assistance with everything I asked for.

My parents deserve special mention for their constant support and prayers. My father, Harish Lalan, is the person who has been most fundamental to my learning character, showing me the joy of intellectual pursuit ever since I was a child. My mother, Bharati Lalan, is the one who sincerely raised me with her caring and love. Last but not least, I thank God for the wisdom and perseverance that He has bestowed upon me during this research project, and indeed, throughout my life.

I dedicate this thesis to my mother and father.

ABSTRACT

Author: Harshad H. Lalan
Title: Guidance, Navigation and Control of a Fly-By-Wire Transport Category Airship designed for Hover Cargo Delivery
Institution: Embry-Riddle Aeronautical University
Degree: Master of Science in Aerospace Engineering
Year: 2009 – 2011

The purpose of this thesis is to develop fly-by-wire pilot controls for a transport category airship propelled with six thrust vectoring engines, and to develop control laws to maintain position, heading, and attitude during hover and cargo operations. Owing to the large body area, most airships require that they be pointed into the wind to maintain their position. This research aims at controlling an airship attitude and position during hover cargo delivery, irrespective of the wind direction.

Control laws were developed for two primary modes of the airship: Flight (High Speed Mode) and Hover (Cargo Delivery Mode). Different sets of pilot controls were developed for each mode, oriented towards reduced pilot work load and simplicity of operation. A proof of concept sub-scale model of the airship was built and flown in an indoor hangar environment. An Attitude Heading Reference System (AHRS) system was implemented using Inertial Measuring Unit (IMU) and a Magnetometer. Indoor positioning of the airship was achieved using target LEDs, and applying robotic vision techniques such as motion detection, color blob analysis, and stereo vision. The developed control laws were tested during indoor flight tests, and conclusions were drawn regarding their feasibility.

1. INTRODUCTION.....	13
1.1 HISTORY OF AIRSHIPS.....	13
1.1.1 <i>Birth of Lighter-than-air Flight</i>	13
1.1.2 <i>Birth of Airships</i>	13
1.1.3 <i>The Golden Age</i>	14
1.1.4 <i>Modern Use of Airships</i>	15
1.2 FLY-BY-WIRE CONTROL BACKGROUND.....	15
1.3 STEREO VISION BACKGROUND.....	16
2. SCOPE AND APPLICABILITY.....	17
2.1 SIGN CONVENTIONS.....	17
2.2 STRUCTURAL SETUP.....	19
2.3 PROPULSION SETUP.....	20
2.4 PILOT CONTROLS.....	22
2.5 MISSION PROFILE.....	22
2.6 MODEL ASSUMPTIONS.....	23
3. METHODS.....	24
3.1 TOP LEVEL DESIGN.....	24
3.2 CONTROL SYSTEM BLOCK (CSB).....	25
3.2.1 <i>Low Speed Sub-system (CSB)</i>	27
3.2.2 <i>High Speed Sub-system (CSB)</i>	28
3.2.3 <i>Roll Stabilization</i>	30
3.2.4 <i>Pitch Stabilization</i>	31
3.2.5 <i>Position Hold Sub-system</i>	31
3.2.6 <i>Heading Hold Sub-system</i>	33
3.2.7 <i>Ballonet System</i>	34
3.3 GRAPHICAL USER INTERFACE (GUI).....	36
3.4 SERVO AND MOTOR COMMAND.....	38
3.5 JOYSTICK (USER INPUT).....	39
3.6 NAVIGATION/POSITION SOLUTION.....	40
3.6.1 <i>Intrinsic and Extrinsic Parameters</i>	41
3.6.2 <i>Camera Calibration and Setup</i>	45
3.6.3 <i>Solving the Correspondence Problem</i>	50
3.6.4 <i>Vision Filters</i>	51
3.6.5 <i>Stereo Triangulation</i>	55
3.6.6 <i>Axis Transformations</i>	55
3.6.7 <i>Position Error Calculations</i>	56
3.7 ATTITUDE HEADING REFERENCE SYSTEM (AHRS) SOLUTION.....	58
3.7.1 <i>Inertial Measuring Unit (IMU) and Magnetometer</i>	58
3.7.2 <i>Kalman Filter Implementation</i>	58
3.8 COMMUNICATION AND ACTUATION.....	59
4. RESULTS AND ANALYSIS.....	61
4.1 ATTITUDE HEADING REFERENCE SYSTEM (AHRS) RESULTS.....	61

4.2 VISION POSITION SYSTEM RESULTS.....	63
4.3 CONTROL SYSTEM RESULTS	65
5. CONCLUSION AND RECOMMENDATIONS.....	68
5.1 FUTURE WORK	68
6. REFERENCES.....	69
7. APPENDIX A: PRINTED CIRCUIT BOARD (PCB) DESIGN.....	70

LIST OF TABLES

Table 1: Dimensions for the Single-Hull Configuration.....	19
Table 2: Dimensions for the Sub-Scale Model	19
Table 3: Engine Identification	20
Table 4: Airship Modes	25
Table 5: Mode Selection Lookup Table.....	25
Table 6: Servo and Motor Command.....	38
Table 7: AHRS Accuracy Results.....	61
Table 8: Vision Position System Error	63

LIST OF FIGURES

Figure 1: Positives Sense Definition for Single Hull Airship.....	17
Figure 2: Engine positive sense of direction.....	18
Figure 3: DATUM definition for the Single Hull Airship.....	18
Figure 4: Engine Location in the YZ plane	19
Figure 5: Engine ID and Locations.....	20
Figure 6: 2 Axis Gimbals System	21
Figure 7: Saitek Aviator Joystick.....	22
Figure 8: Airspeed Envelope	23
Figure 9: Top-Level System Architecture	24
Figure 10: CSB Top-Level Design	26
Figure 11: Low Speed Control Logic	27
Figure 12: Low-Speed Mode Joystick Control Configuration	28
Figure 13: High Speed Control Logic.....	29
Figure 14: High Speed Mode Joystick Control Configuration	30
Figure 15: Low Speed Roll Controller	30
Figure 16: Low Speed Pitch Controller	31
Figure 17: Position Hold Sub-System.....	32
Figure 18: Position Hold Throttle Controller.....	32
Figure 19: Position Hold Vector Controller.....	33
Figure 20: Heading Hold Block.....	33
Figure 21: Heading Hold Sub-System	34
Figure 22: Ballonet Trim Controller Block	36
Figure 23: Engine Orientation and Throttle Display	37
Figure 24: Airship Attitude Orientation.....	37
Figure 25: Instrument Cluster	37
Figure 26: Airship Display System.....	38
Figure 27: Command Packets	39
Figure 28: Joystick Interface.....	40
Figure 29: Position Solution Process	41
Figure 30: Dynex™ 1.3MP Webcam	41
Figure 31: Check Board Reference Frame.....	44
Figure 32: Uncalibrated Images.....	45
Figure 33: Manual Corner Extraction	46
Figure 34: Extracting Grid Corners	46
Figure 35: World Centered View.....	47
Figure 36: Camera-Centered View	47
Figure 37: Pixel Projection Error.....	48
Figure 38: Tangential Distortion Model	49
Figure 39: Radial Distortion Model.....	49
Figure 40: Complete Distortion Model.....	50
Figure 41: Onboard LED Target.....	51
Figure 42: LED Circuit.....	51
Figure 43: Right Camera Block	51
Figure 44: Background Estimation Filter	52

Figure 45: Background Estimators	53
Figure 46: Color Analysis.....	53
Figure 47: Pixel Reference System.....	54
Figure 48: Blob Analysis	54
Figure 49: Stereo Triangulation	55
Figure 50: 3D Position Coordinate Transformations.....	56
Figure 51: Position Error Coordinate Transformations	57
Figure 52: Spark Fun Atomic Magnetometer	58
Figure 53: Kalman Filter.....	59
Figure 54: System Communication Overview.....	60
Figure 55: AHRS Results.....	62
Figure 56: Vision System Error Analysis	64
Figure 57: Airship in Flight # 1	66
Figure 58: Airship in Flight # 2	67

LIST OF ACRONYMS

ERAU	Embry-Riddle Aeronautical University
AHRS	Attitude Heading Reference System
BE	Bow Engine
CG	Center of Gravity
CSB	Control System Block
CV	Center of Volume
ERAU	Embry-Riddle Aeronautical University
GPS	Ground Positioning System
GUI	Graphical User Interface
IMU	Inertial Measuring Unit
LED	Light Emitting Diode
PA	Port Aft
PF	Port Forward
PID	Proportional, Integral and Derivative
SA	Starboard Aft
SF	Starboard Forward
TE	Tail Engine

NOMENCLATURE

α	Angle of attack
f_c	Focal Length
cc	Principal Point
α_c	Skew Coefficient
k_c	Distortions
x_n	Normalized (pinhole) image projection
dx	Tangential Distortion Vector
KK	Camera Matrix
O	Origin

1. INTRODUCTION

The purpose of this thesis is to develop fly-by-wire pilot controls for a transport category airship. Airships in general have a large surface area, and, as a result, are very hard to control in windy conditions. Today, one of the most sought-after applications of airships is to use them for transporting cargo over long distances and harsh terrain. While loading/unloading certain cargo, it's essential that the airship maintains its position and direction, irrespective of the weather conditions. This research focuses on developing control laws to control such an airship and test these control laws on a proof-of-concept sub-scale model. A brief history of airships and various systems used in this thesis is provided below.

1.1 History of Airships

1.1.1 Birth of Lighter-than-air Flight

Any history of the airship must start with the birth of lighter-than-air travel. This leads us to Roger Bacon, an English scholar of the 13th Century. He set forth a strategy for human powered flight that involved lifting a man with a structure “filled with the thin air of the upper atmosphere, or with liquid fire, thus rising high into the heavens.” This is the first recorded theory for lighter than air travel.

In 1783, two French brothers, Jacques Etienne and Joseph Michel Montgolfier, invented the hot-air balloon and sent one to an altitude of 6,000 ft (1,800m). Later that year, the French physicist Jean Pilatre de Rozier made the first manned balloon flight. While balloons could travel to high elevations, they could not travel on their own propulsion and were at the mercy of the prevailing winds. The attempt to control the direction and velocity of these balloons led to the birth of the “Airship.”

1.1.2 Birth of Airships

An Englishman named Baron Scott first laid down an airship design in 1789. The design included two ballonets that could inflate and deflate to control the attitude of the airship. In 1843, Monk Mason of Great Britain made a model of an airship powered by a clockwork engine, and

attained speeds of several miles per hour. An Austrian named Paul Haenlein build the first full sized powered dirigible ship and flew it on December 13th, 1872. A year later, Count Ferdinand von Zeppelin designed the first airship with separate gas cells, all filled with hydrogen. This became the trademark of Zeppelin designs until the last ship was produced. The first airship he built, LZ1, was a failure. The twin 16 HP engines did not have enough power to overcome strong winds. The second airship, LZ2, was better designed, and had an even more powerful propulsion system. LZ2 was destroyed in an overnight storm. LZ3 was the first successful airship, and flew on October 9th, 1906. The LZ3 was designed based on lessons learned from the mistakes of LZ1 and LZ2 and received orders from the German military. Zeppelins were used in the First World War as the first long range bombers. The Zeppelins were also used extensively for transportation of armament to German troops at the frontline. At the end of the First World War, the Zeppelins were destroyed or given as war reparations.

1.1.3 The Golden Age

The golden age of the airship started after the First World War, when many of the allied nations decided to invest in building airships. The golden age is marked by some of the very famous airships such as the Shenandoah, the Los Angeles, the Graf Zeppelin, the Akron, the Mason, and the Hindenburg. The Shenandoah was a US navy aircraft carrier of the sky and the first rigid airship built in the United States. The Shenandoah was destroyed in a storm killing 14 crewmen. The Los Angeles was then the only airship under the US arsenal after the Shenandoah was destroyed. The Los Angeles used Helium for safety and was the only airship to survive until decommissioned in 1939. The Graf Zeppelin (LZ128) made its first flight on September 18th, 1928. It was the first airship to go around the world in 21 days, and logged more than one million miles of flight. The success of LZ128 led to the development of even bigger airship, the Hindenberg. The Akron and the Mason were two military airships, built by Goodyear and Zeppelin respectively. The USS Akron served as a flying aircraft carrier, launching Sparrowhawk biplanes. On May 6th, 1937, the Hindenburg burst into flames while landing at Lakehurst, New Jersey. The accident killed 35 people, marking the end of the Golden Age of airships. Although the disasters of airships are highlighted, non-rigid airships have by far the best safety record of any type of flying vehicle.

1.1.4 Modern Use of Airships

Because lighter-than-air gas provides the lift in an airship or blimp, rather than a wing with an engine as in an airplane, airships can fly and hover without expending fuel or energy. Furthermore, airships can stay aloft anywhere from hours to days; much longer than airplanes or helicopters. These properties make them ideal for such uses as covering sporting events, advertising, and some research, such as scouting for whales.

Recently, there has been renewed interest in using rigid airships for lifting and/or transporting heavy cargo loads—like ships, tanks, and oil rigs—for military and civilian purposes. Modern airships, such as the Zeppelin NT and CargoLifter, use lightweight, carbon-composite frames that allow them to be huge, light and structurally sound. There has been a large standing need in both commercial and governmental applications for airships that can pick up very large, indivisible objects and transport them over long distances. In certain areas, such as Alaska and Canada, harsh arctic conditions and the lack of transportation infrastructure frustrate development. Airships represent a unique solution to many of these transportation challenges.

1.2 Fly-By-Wire Control Background

A fly-by-wire system is an electronic interface that substitutes the traditional mechanical and hydraulic flight controls. Instead of mechanical linkages between the pilot controls and actuators, the pilot commands are converted into digital signals transmitted by wires to the actuators. Fly-by-wire systems considerably reduce weight and complexity.

Controlling actuators using electronic signals was first tested in the 1950s. The first non-experimental aircraft to fly with a fly-by-wire flight control system was the Avro Canada CF-105 Arrow in 1958. [1] The first digital fly-by-wire aircraft to fly was an F-8 Crusader in 1972, which was modified by NASA as a test aircraft. The same concept was employed by the USSR in the Sukhoi T-4, and by the United Kingdom in the Hawker Hunter. During 1984, the Airbus

A320 became the first airliner to fly with an all-digital fly-by-wire control system. In 2005, the Dassault Falcon 7X became the first business jet to use a fly-by-wire flight control system.

1.3 Stereo Vision Background

Stereo vision is one of several techniques in which we recover depth information from two images that depict the scene from different perspectives. The theory of depth from stereo has been well understood for years, while the engineering challenge of creating a practical stereo sensor has been formidable. Stereo vision has a lot of applications in automated systems and robotics. It is mostly used for range sensing, object recognition, contour maps, etc. There is no standard formulation of how computer vision problems should be solved. There are many methods available for solving various well-defined computer vision tasks, where the methods often are very task specific and seldom can be generalized over a wide range of applications. Many of the methods and applications are still in the state of basic research, but more and more methods have found their way into commercial products.

2. SCOPE AND APPLICABILITY

2.1 Sign Conventions

A positive sense of directions and rates are specified and used throughout the design process. As far as practically possible, the same conventions have been kept as used for general aviation. The following figure shows the positive sense of direction, rates and surface deflection. From the figure looking out the cockpit: a roll to the right, pitch up, and yaw to the right are considered positive.

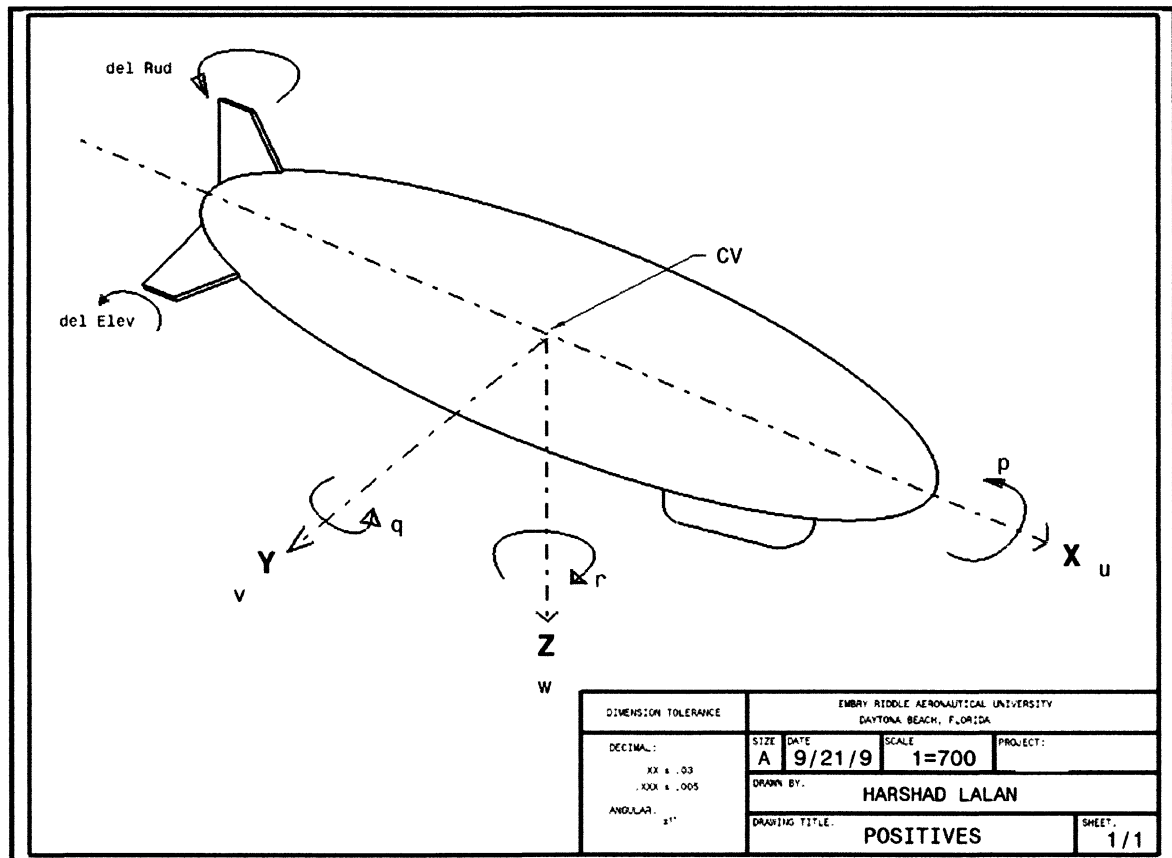


Figure 1: Positives Sense Definition for Single Hull Airship

The X, Y, and Z axis meet at the Center of Volume (CV) contrary to the Center of Gravity (CG), which is normally used for general aviation airplanes. Since the propulsion system will be thrust vectored, their positives are also defined. The thrust of the tail lateral propeller is considered positive in the '+' Y axis direction. The following figure shows the positive sense for the engine swivel in the XZ plane.

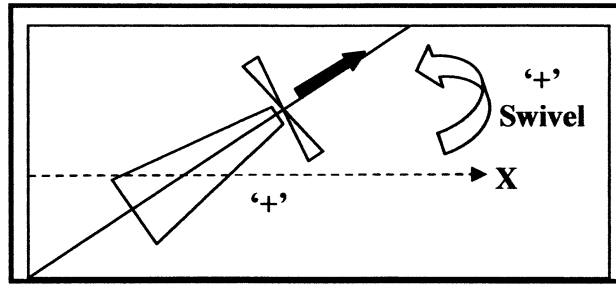


Figure 2: Engine positive sense of direction

The following figure defines the datum used. From the figure, the XY Datum is defined as 100 feet below the bow stern center line. The YZ Datum is located at the nose of the airship and the XZ Datum passes through the center of the airship.

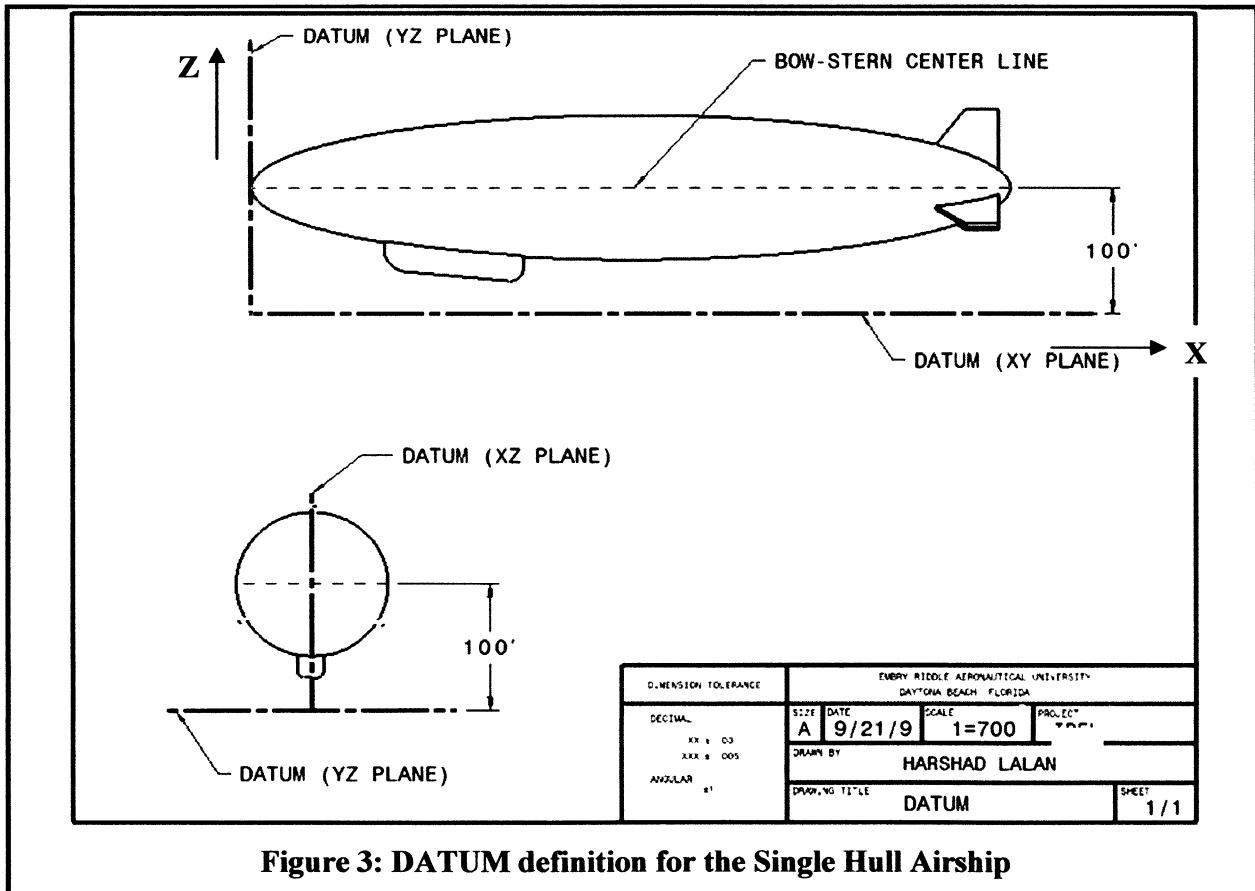


Figure 3: DATUM definition for the Single Hull Airship

2.2 Structural Setup

The following tables list some of the basic dimensions of the proposed Single-Hull Airship, and those of the proof-of-concept model.

Table 1: Dimensions for the Single-Hull Configuration

Length	168.25 m	552 ft
Maximum Diameter	33.53 m	110 ft
Total Volume	112,049.76 m ³	3,957,000 ft ³
Total Weight	50 metric tons	110,231 lb
Max Payload Weight	60 metric tons	132,277 lb

Table 2: Dimensions for the Sub-Scale Model

Length	4.27 m	14 ft
Maximum Diameter	0.6 m	2 ft
Total Volume	1.25 m ³	44 ft ³
Total Weight	2950 grams	6.5 lb
Max Payload Weight	453.6 grams	1 lb

On the full scale proposed airship, the envelope and the engines are supported by a triangular internal frame as shown in figure 4. For the sub-scale model, the same triangular concept is used to support the motors, but, to simplify the building process; the envelope is placed inside the triangular structure.

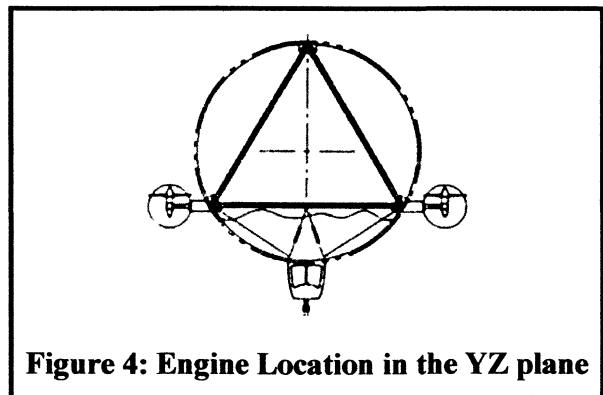


Figure 4: Engine Location in the YZ plane

2.3 Propulsion Setup

A total of six engines are required to meet all maneuver and power needs of the airship. The general arrangement of these six engines is shown in figure 5 and their labels are shown in table 3.

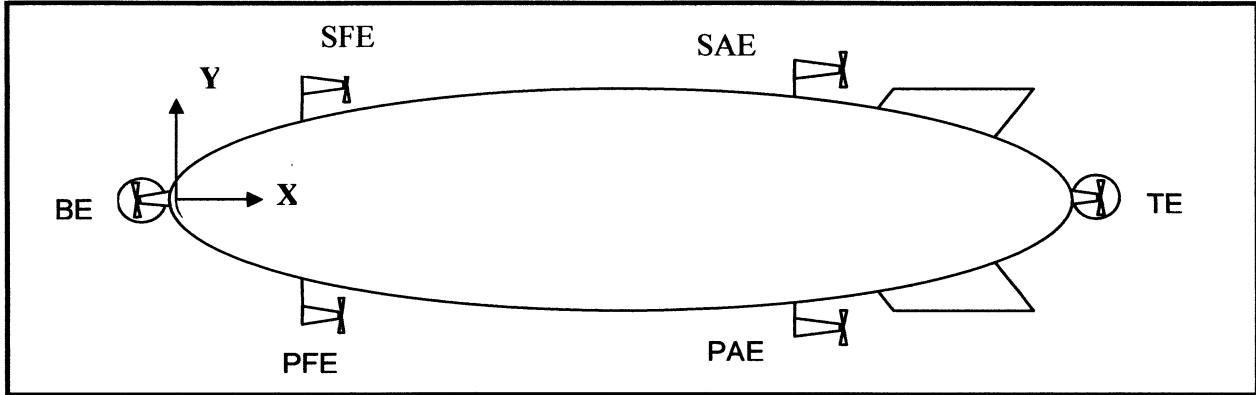


Figure 5: Engine ID and Locations

Table 3: Engine Identification

Engine No.	Engine ID	Engine Location	Swivel
1	PFE	Port Forward	Two-Axis Gimbals
2	SFE	Starboard Forward	
3	PAE	Port Aft	
4	SAE	Starboard Aft	
5	TE	Tail	Single-Axis Gimbals
6	BE	Bow	

As shown in the above table, two types of engines are used on this airship:

- 1) Main Engine X 4
- 2) Tail/ Bow Rotor

The four main engines are located at 25% and 75% of the length of the airship hull. The further away the engines are from the CG of the airship, the more effect their thrusts have on the airship moment. This helps provide quick and very effective control of pitching and yawing moments. On the other hand, the large structure also results in the bending and warping of the structure. This results in error in the effective thrust lines of these engines. For the purpose of this study, this effect is ignored.

Each engine is a pusher type of system, as opposed to a puller system. Hence, the propellers in the figures are shown facing aft. In this configuration, a single propeller engine is mounted in a dual gimbal system. This configuration allows using one propeller setup to provide thrust in all directions. This reduces mechanical complexity while improving maneuverability. Figure 6 shows the two-axis gimbals as applied on the sub-scale model.

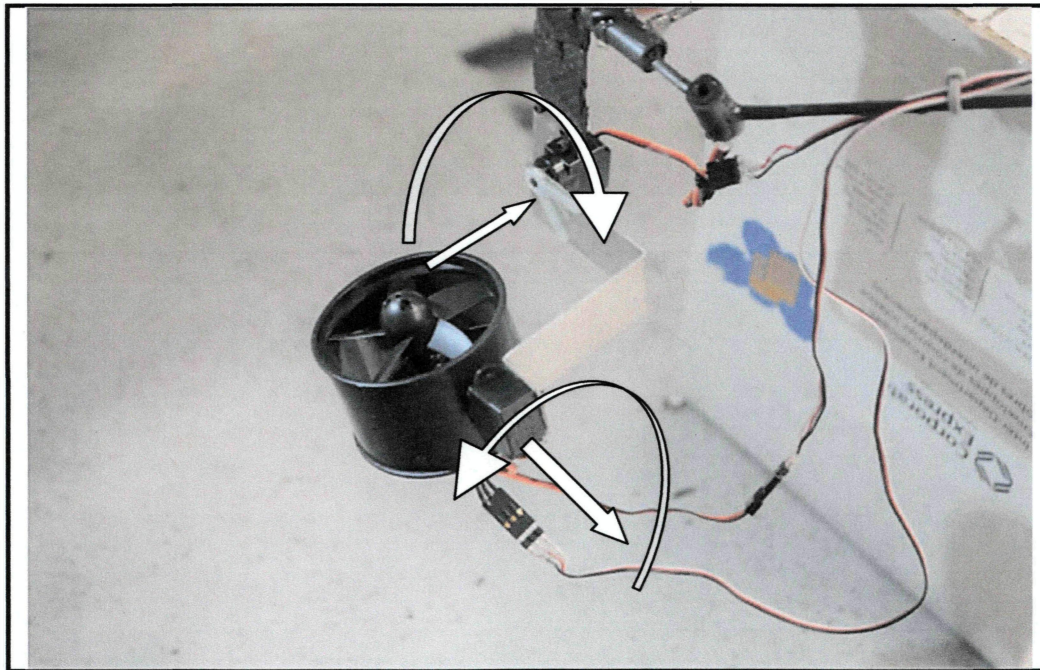


Figure 6: 2 Axis Gimbals System

2.4 Pilot Controls

The pilot controls are designed to provide maximum control of the airship while minimizing pilot load. The controls are designed to be simple and intuitive. A Saitek Aviator Joystick was used to control the airship, as shown in figure 7. The airship controls in hover and low speeds depict that of any conventional helicopter and at high speeds; the airspeed controls depict a conventional aircraft. As a result, there are two basic modes of the airship that will be discussed in detail in later sections.

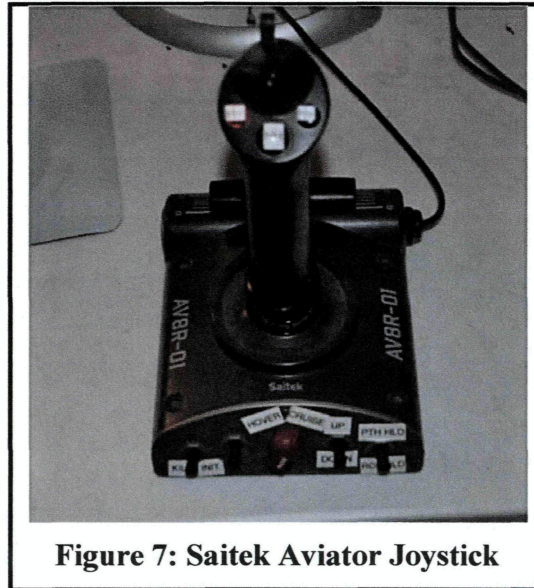


Figure 7: Saitek Aviator Joystick

2.5 Mission Profile

The proposed airship is designed to have a cruising speed of 55 knots and a maximum forward speed of 75 knots. During cargo loading/unloading, it should be able to withstand winds of 20 knots in all directions. These requirement forms the basis of the control law design. This mission profile is best illustrated by figure 8.

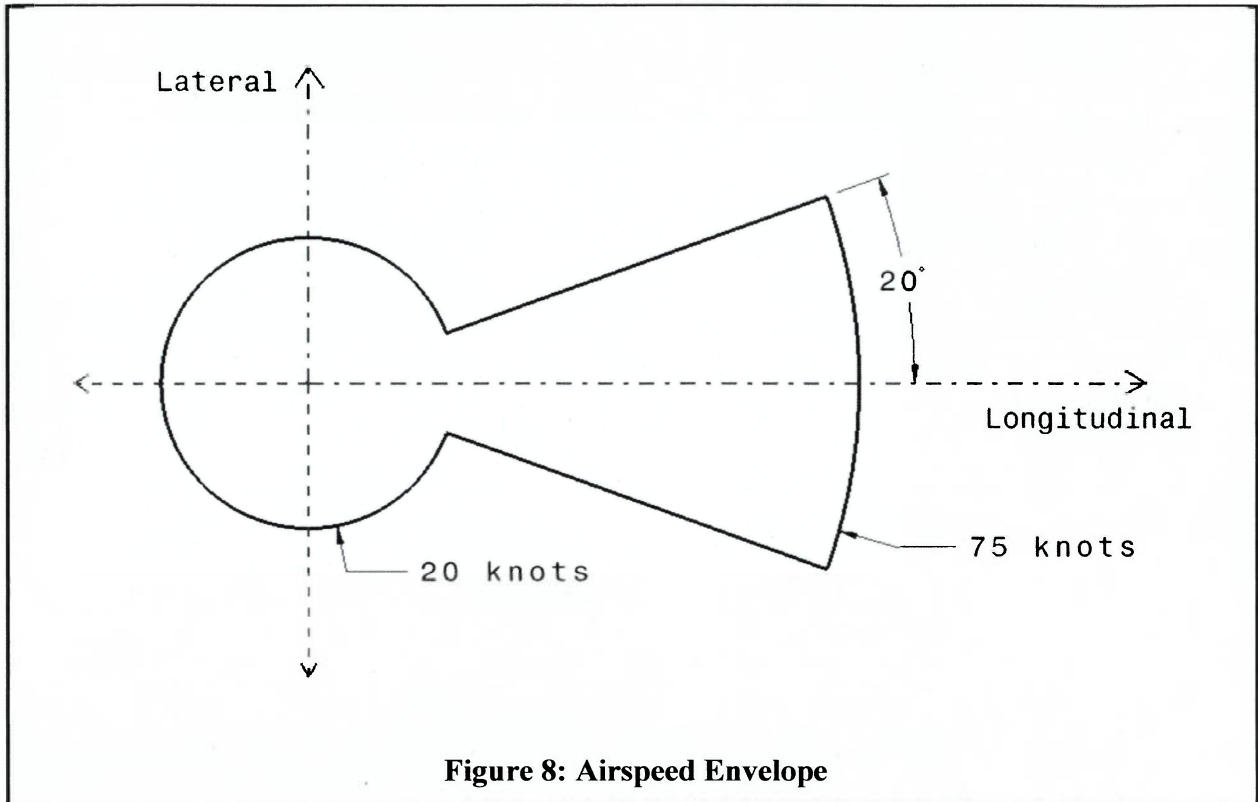


Figure 8: Airspeed Envelope

2.6 Model Assumptions

The following assumptions were made for the purpose of this study.

- 1) The sub-scale model will be flown in an indoor hangar environment where the airspeed will never be more than 20 knots. Hence, all the aerodynamics effects will be ignored including envelop shape, control surface effects, etc.
- 2) The model will be assumed to be rigid, thus ignoring the warping and bending of the structure.
- 3) Ballonets will not be installed and their effects will be ignored.
- 4) Helium pressure will be arbitrary, and will not be actively controlled.
- 5) Effects of temperature and altitude on the helium lift will be ignored.
- 6) Control laws are designed for a slightly negative buoyant airship.

3. METHODS

3.1 Top Level Design

The general structure of the entire system is shown in figure 9.

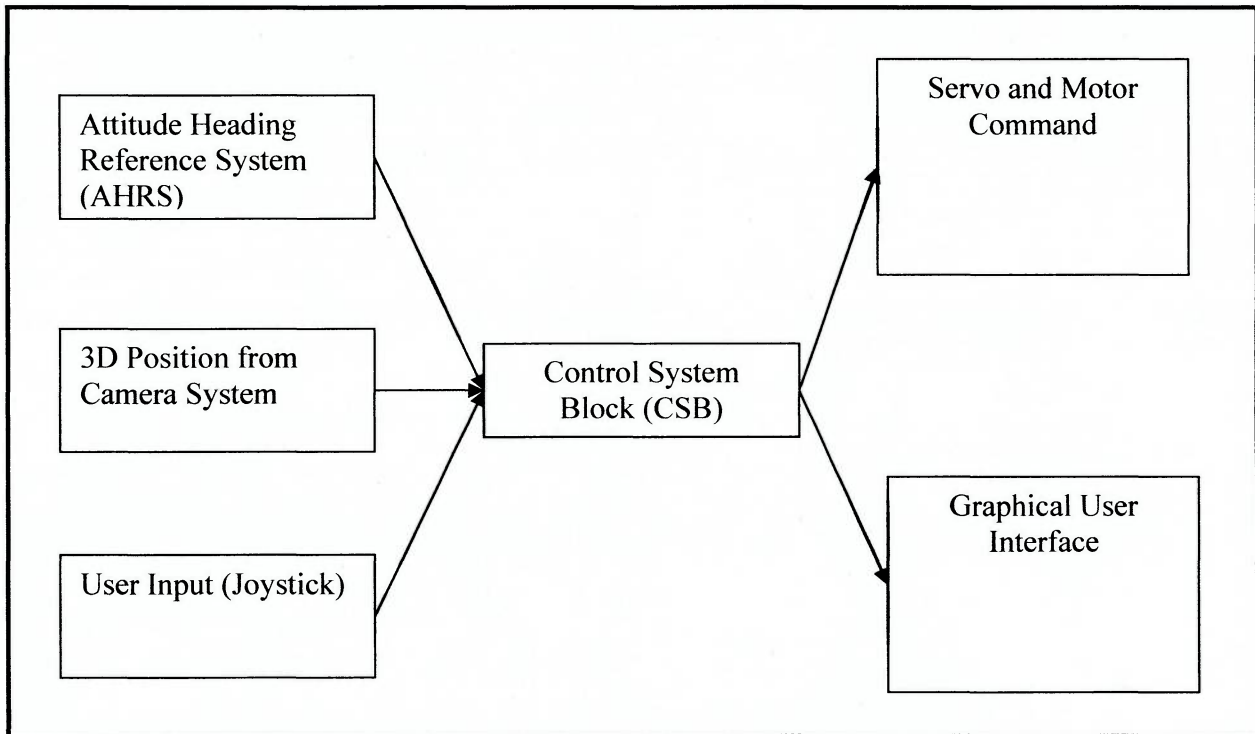


Figure 9: Top-Level System Architecture

The Control System is implemented in the Simulink environment. It receives attitude information from the on-board Attitude Heading Reference System (AHRS). The 3D position of the blimp is provided by the stereo-camera system. The user commands are received through the joystick. The Graphical User Interface (also implemented within Simulink) displays blimp position, attitude information, engine positions, and power settings to the user. The servo and motor control laws are transferred to the blimp wirelessly.

Each of the above sub-systems and their processes are discussed in detail in the following sections.

3.2 Control System Block (CSB)

The primary objective of the Top Level Control System Design was to accommodate the specific mission profile requirement described in section 2.5. To meet the forward velocity requirements, thrust from all engines is required to overcome the airship drag forces. During cargo operations, the hardest task for the airship is to maintain its position during strong cross winds. Owing to these requirements, three different regime of airship operations are considered as shown in table 4.

Table 4: Airship Modes

$-20 \text{ knots} \geq \text{airspeed} \geq 20 \text{ knots}$	LOW SPEED
$20 \text{ knots} > \text{airspeed} > 35 \text{ knots}$	TRANSITION SPEED
$\text{airspeed} \geq 35 \text{ knots}$	HIGH SPEED

The control laws are primarily written for low speed and high speed regime only. In the transition speed regime, both the low speed and high speed regime control laws are used. The effectiveness of low speed/high speed control laws in the transition regime depends on the indicated airspeed and is governed by the lookup table 5.

Table 5: Mode Selection Lookup Table

Airspeed(knots)	High Speed (%)	Low Speed (%)
-20	0	100
-15	0	100
-10	0	100
-5	0	100
0	0	100
5	0	100
10	0	100
15	0	100
20	0	100
25	25	75
30	75	25
35	100	0
40	100	0

For the sub-scale model, airspeed is irrelevant as mentioned in section 2.6. Hence the change of modes is governed by a manual switch, as opposed to being airspeed dependent. Also, the transition block is not implemented for the subscale model.

The following figure shows the implementation of the Control System Block as discussed. The FCS block includes three main sub-systems:

- 1) Low Speed Mode Sub-system (orange)
- 2) High Speed Mode Sub-system (cyan)
- 3) Mode Selector (green)

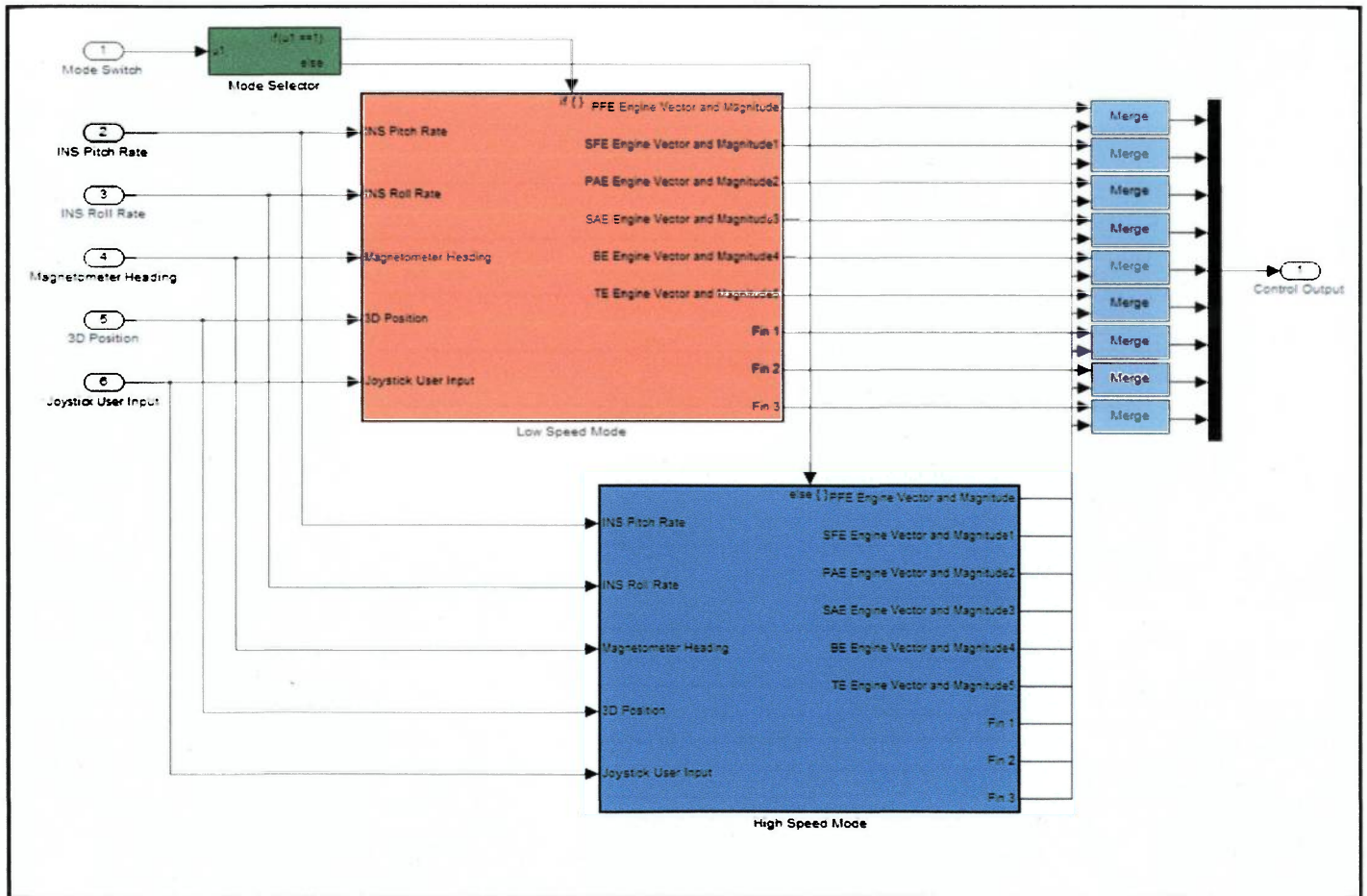


Figure 10: CSB Top-Level Design

3.2.1 Low Speed Sub-system (CSB)

This sub-system has various controls for airship at low speeds and hover mode. At low speeds, there is not enough dynamic pressure on the control surfaces to provide control power. Hence, the fins are locked out. All the control actuation is provided by the four main engines, the tail, and the bow engines. The following figure shows the basic logic implied by this sub-system.

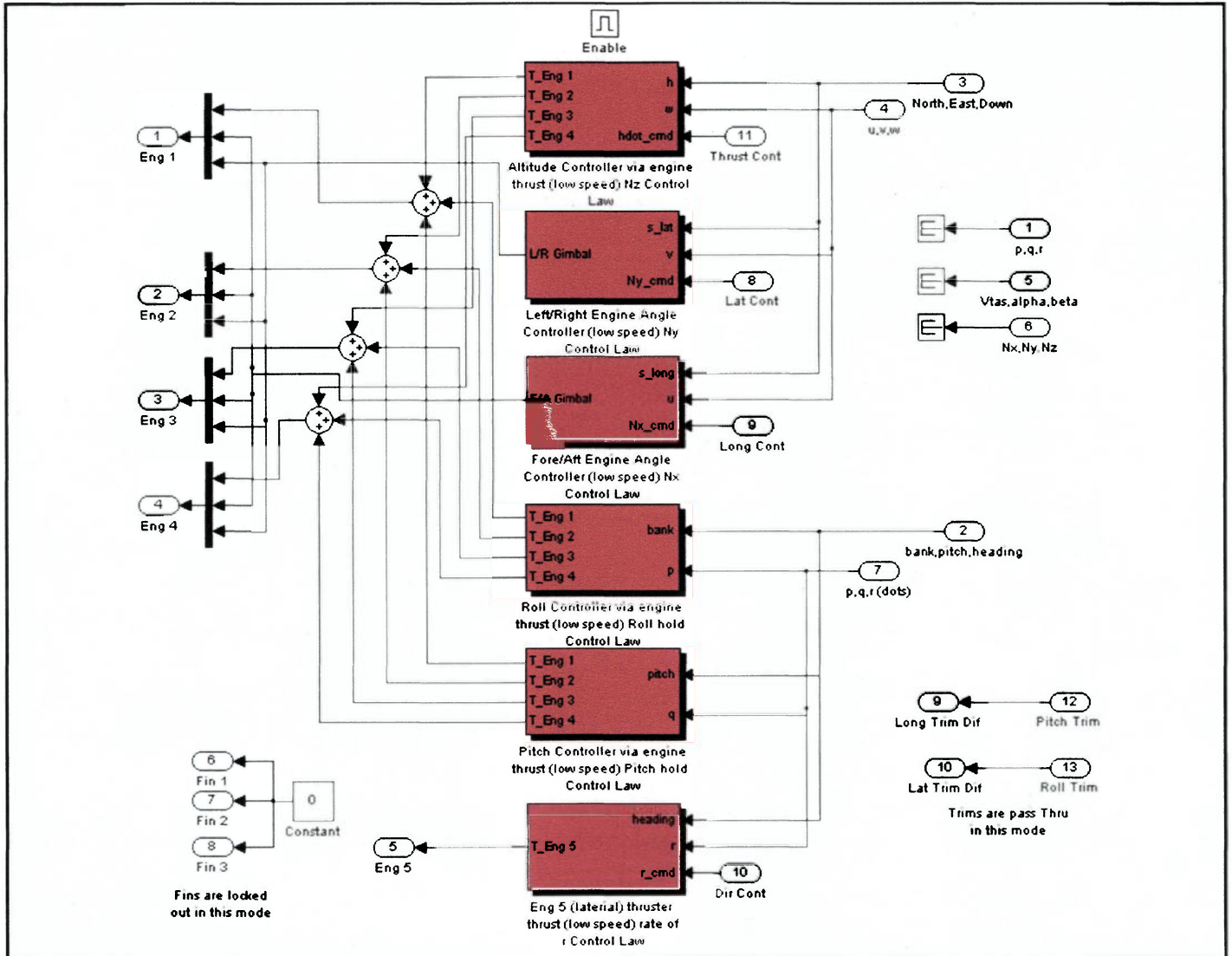


Figure 11: Low Speed Control Logic

The pilot controls in this mode mimic the controls of a helicopter. The basic maneuvers augmented by joystick in this mode are shown in figure on the following page. In this mode, autopilot is engaged for pitch stabilization and roll stabilization. Hence, the airship maintains level attitude at all times.

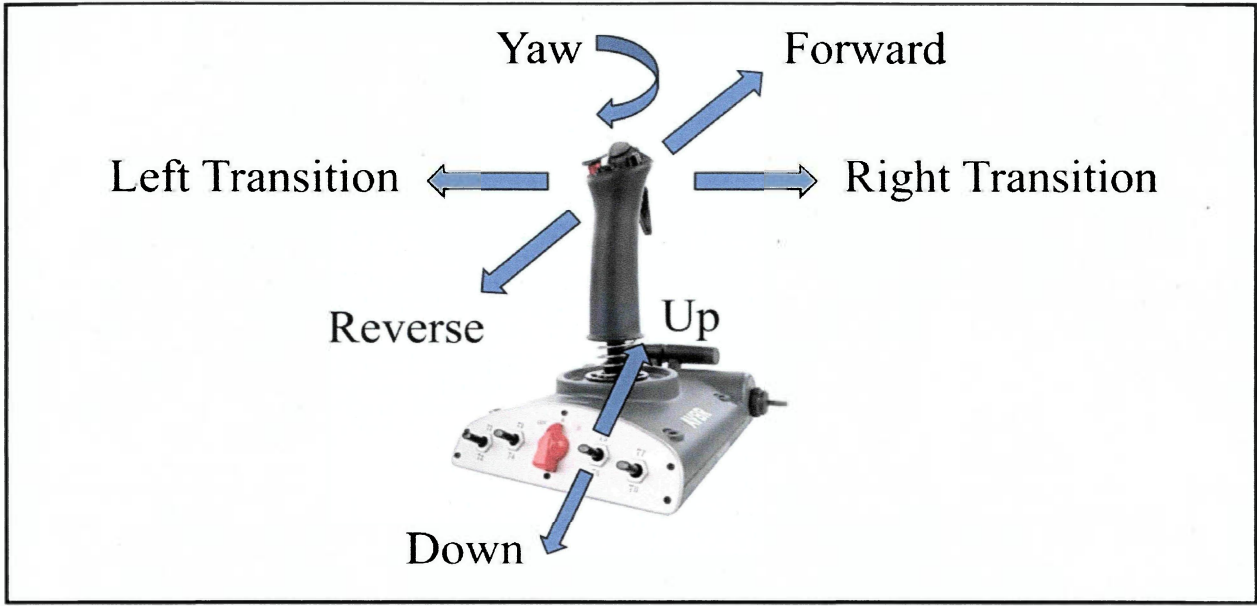


Figure 12: Low-Speed Mode Joystick Control Configuration

In this mode, all the main engines point in the positive Z direction by default. Following joystick command, all motors point thrust in the same direction at a fixed thrust rating.

3.2.2 High Speed Sub-system (CSB)

The high speed control laws are applied at speeds higher than 35 knots and partially implemented during the transition regime (20 knots to 35 knots). The high speed control laws are designed to make the airship behave and control like an airplane. In high speed mode, the engines are primarily used for forward thrust and fins are used for actuation as shown in the logic diagram on the following page. In this mode, all motors point thrust in positive X direction by default. Roll and pitch stimulation is achieved by differential thrust.

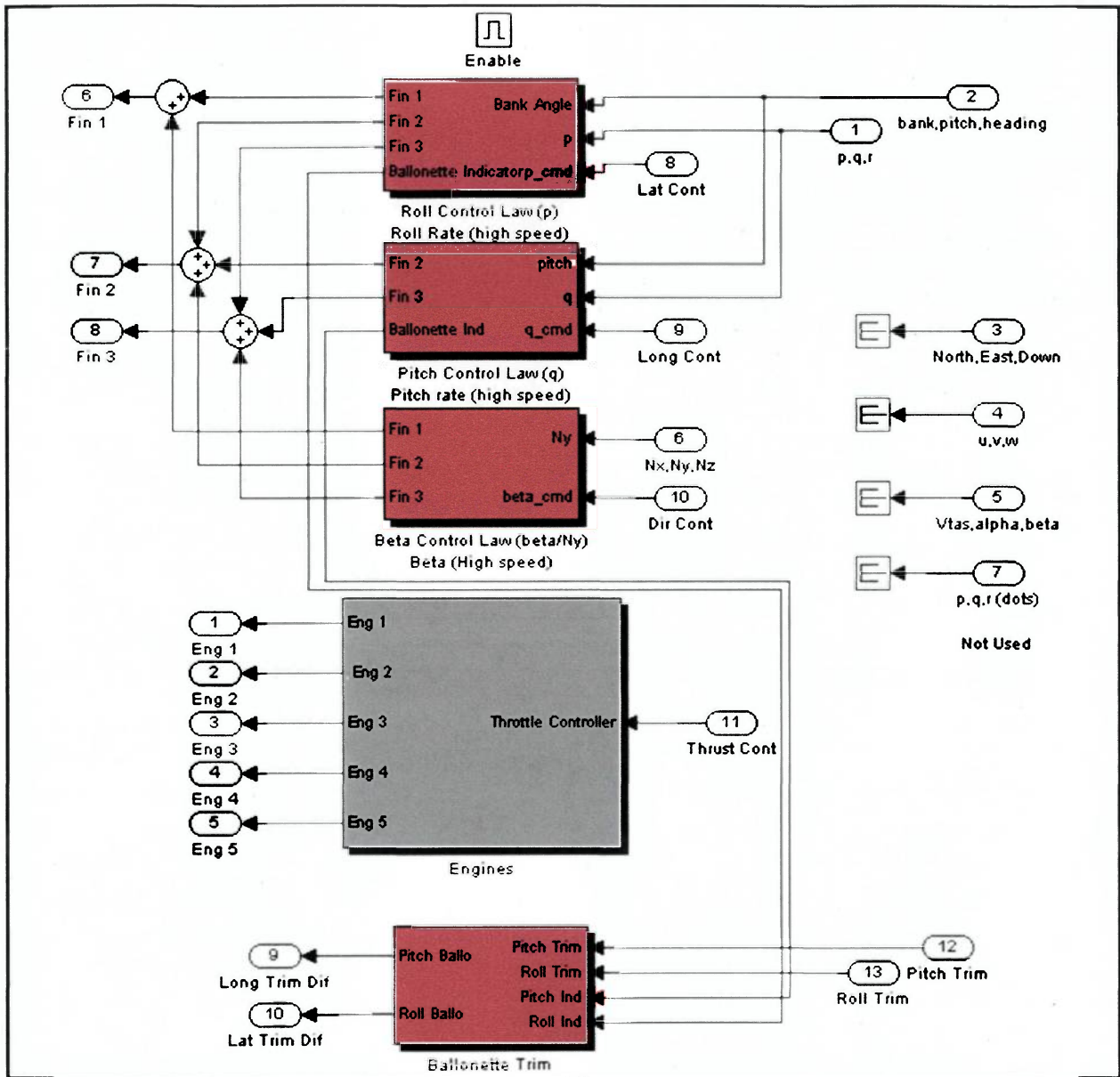


Figure 13: High Speed Control Logic

To test the high speed control laws at low speeds using the sub-scale model the fin actuation is generated by differential engine thrust. For example, to achieve pitch up attitude the two forward engines are rotated along Z axis while keeping the rear engines pointing in the positive X direction.

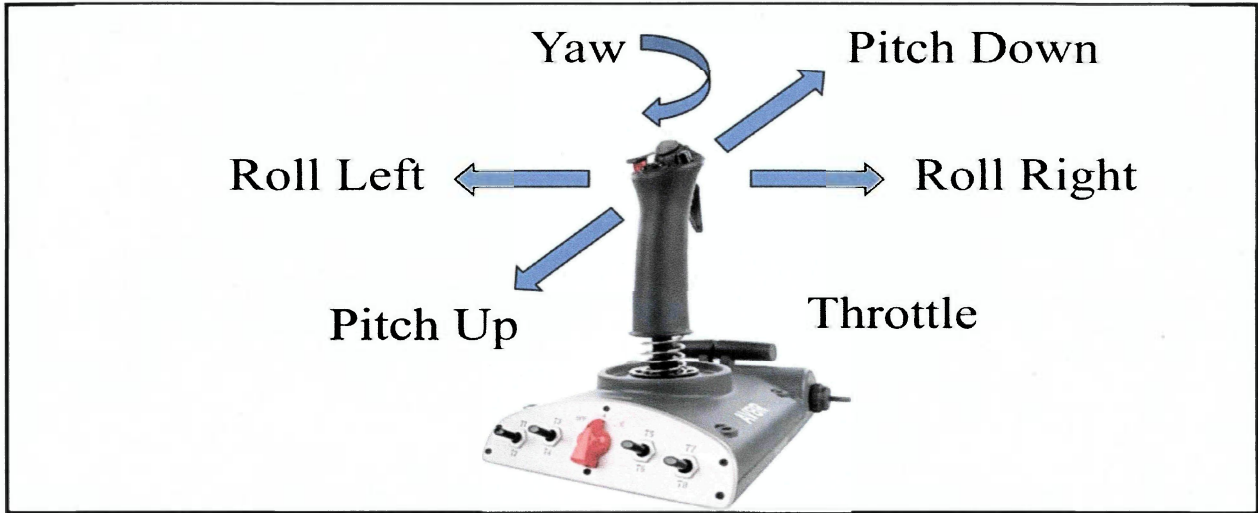


Figure 14: High Speed Mode Joystick Control Configuration

3.2.3 Roll Stabilization

In low speed mode, no pilot input is available to change the roll attitude of the airship. In high speed mode, roll stabilization can be manually turned on/off. For roll stabilization, the controller receives airship bank angle from the processed IMU data. Figure 15 shows the controller logic. The gain values shown in figure 15 were experimentally adjusted for best performance.

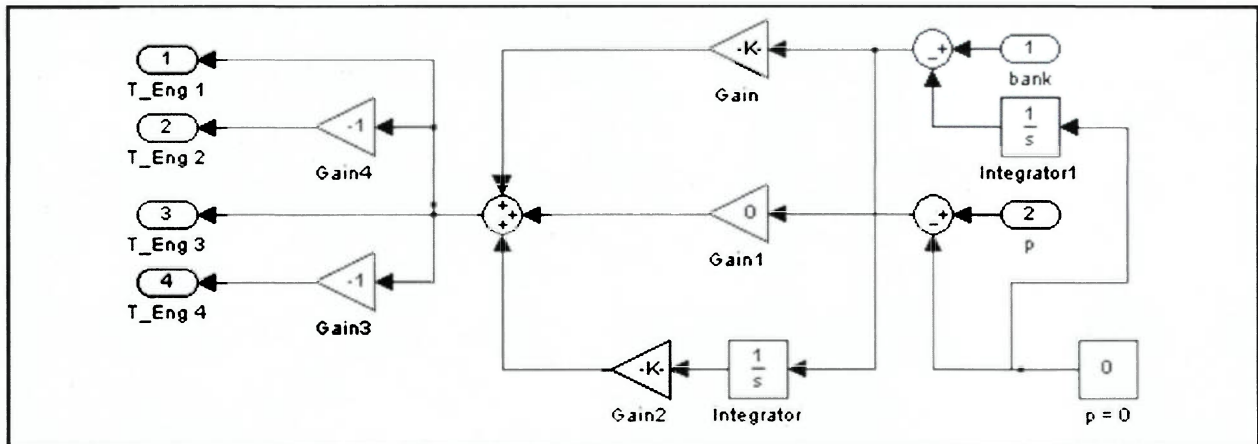


Figure 15: Low Speed Roll Controller

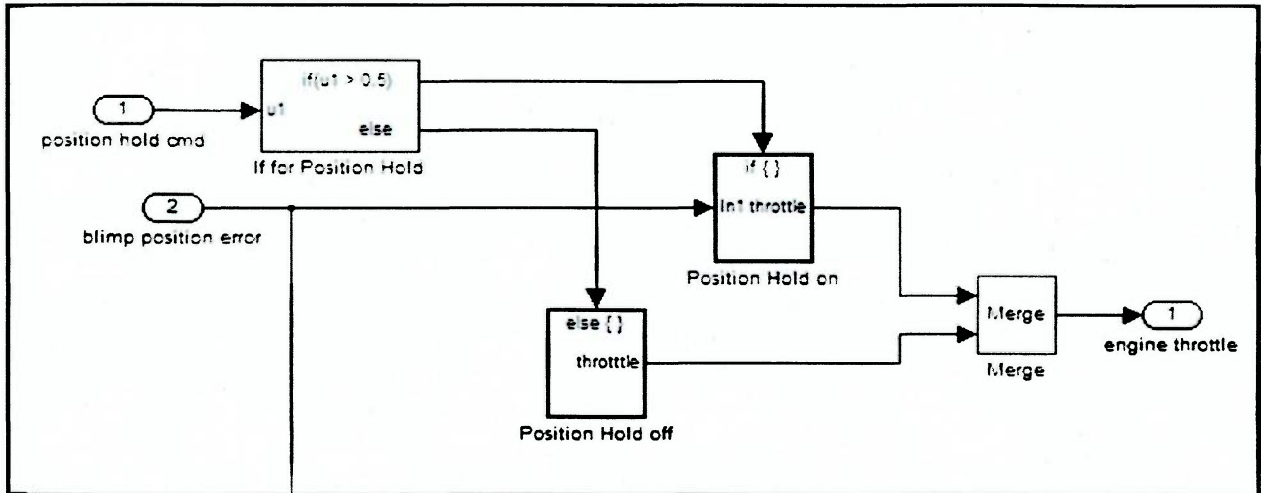


Figure 17: Position Hold Sub-System

When the position hold command is active, the position error is first converted into a range value. A PID controller is then used to regulate the throttle output based on the distance of the current airship position from the target position. A dead zone of 2 ft is also implemented which avoids confusion when the target location is acquired. When the position hold is deactivated, there is no effect on the engine throttle.

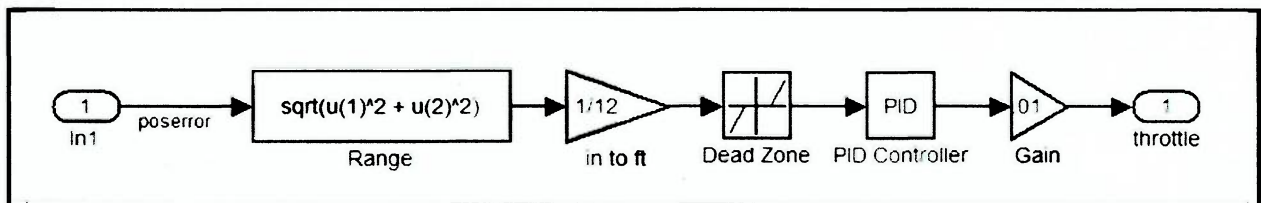


Figure 18: Position Hold Throttle Controller

At the same time, the appropriate thrust vector for each main engine is also calculated as shown in figure below. Based on the status of the position hold command, the subsystem either outputs direct pilot commands or the calculated position correction vector.

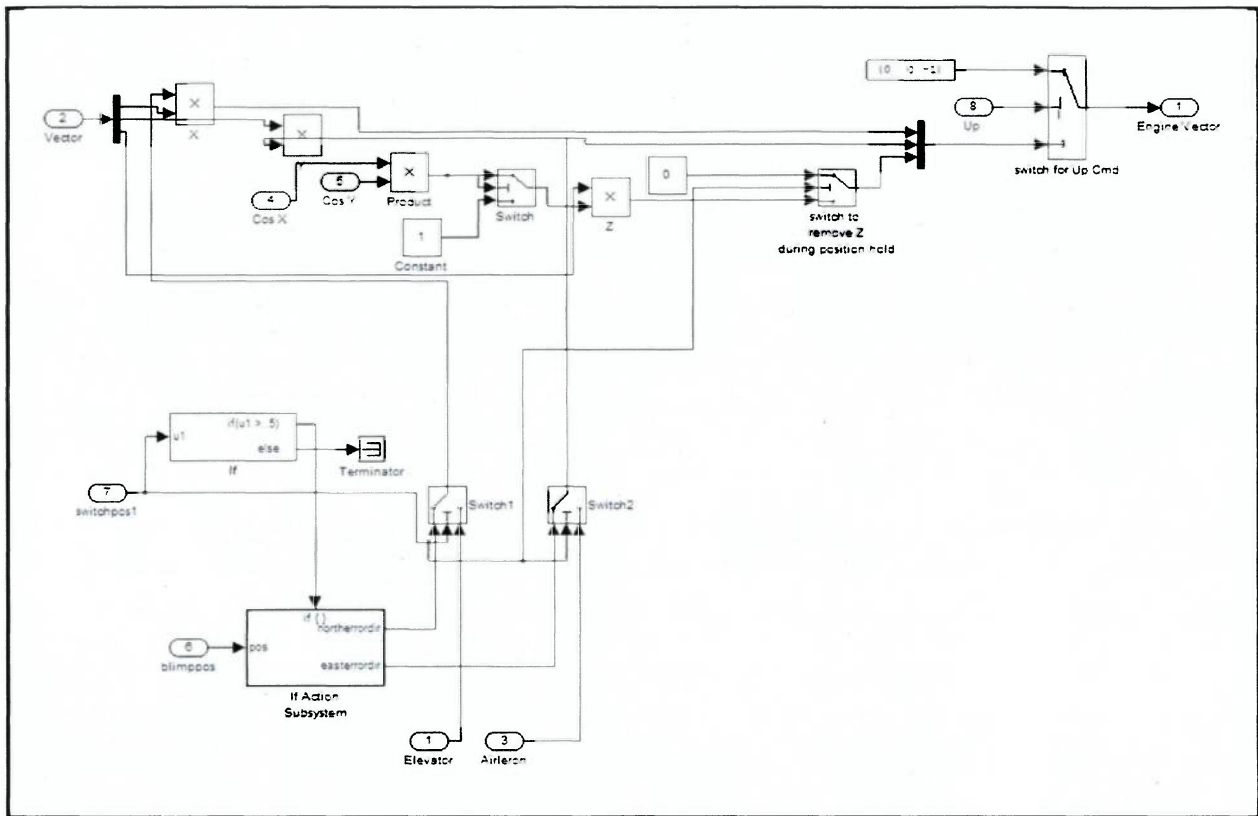


Figure 19: Position Hold Vector Controller

3.2.6 Heading Hold Sub-system

The onboard magnetometer facilitates the need to hold a particular magnetic heading. The airship yaw is only controlled by the bow and tail engines. Only the bow and tail engines are used as they provide the maximum moment because of their further distance from the center of gravity. The heading hold subsystem first calculates the heading error and then creates a appropriate feedback control to capture the desired heading. The top level heading block is shown below:

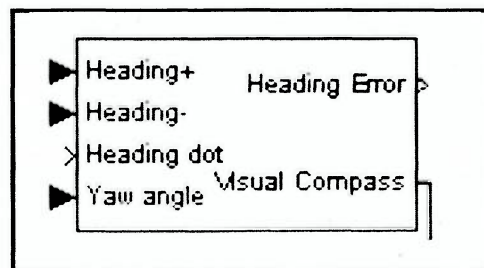


Figure 20: Heading Hold Block

The airship heading is calculated by the AHRS sub-system. The target heading is adjusted by the user using the joystick. The target heading is adjusted in five degree increments using the '+' and

'-' keys on the joystick. This is achieved by a counter that is connected to the joystick input. The heading error is simply the difference between the actual and target heading. There is a ten degree hysteresis designed into the system to reduce heading confusion. When heading error is within the hysteresis range, the heading error computations are removed and replaced by the yaw signal from the joystick. This implementation is shown in the figure below:

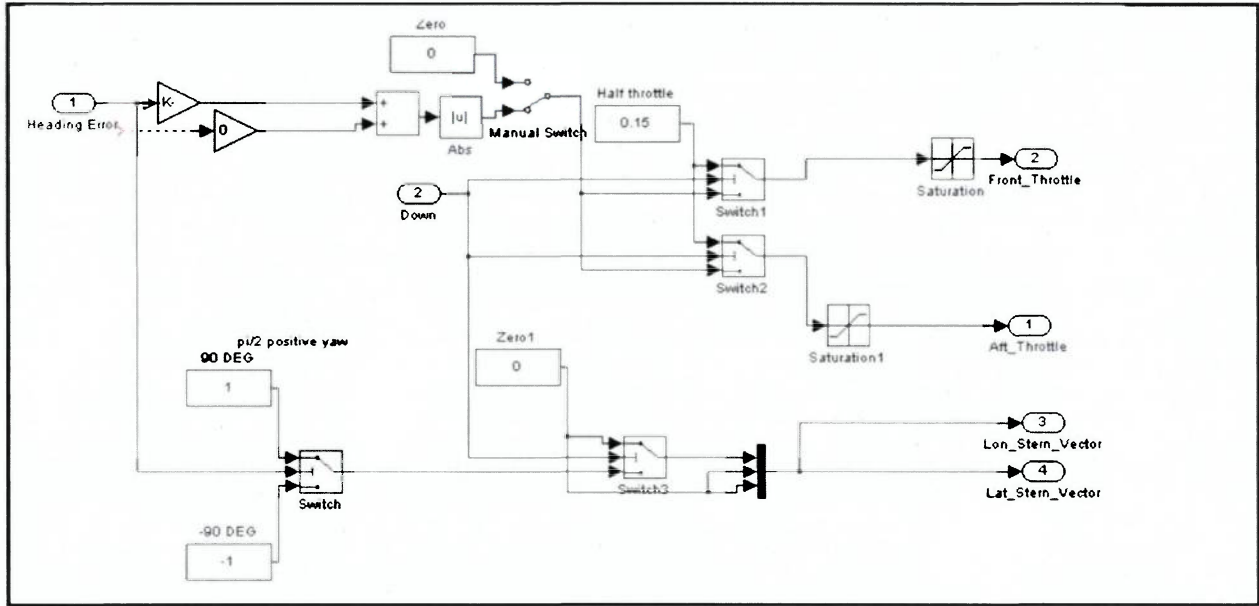


Figure 21: Heading Hold Sub-System

The above system also calculates the shorted travel to the target heading. Based on this calculation, the motors either create a positive or a negative yaw moment. A PID controller is then used to regulate the throttle of the bow and tail motors. The PID controller is adjusted to create a critically damped system.

3.2.7 Ballonet System

This airship is also designed to use dynamic lift and thrust to control altitude of the airship. The buoyancy of these airships is controlled by controlling the ballonet volumes within the airship. Ballonets also help maintain the shape of the envelope by automatically adjusting themselves with changing altitude. The internal pressure within the airship envelop is maintained at a slightly higher pressure than the corresponding outside atmospheric pressure. This helps to maintain tension in the airship envelop and maintain its hull shape. As the altitude of the airship

increases, the temperature of the atmosphere drops and the volume of the helium increases. Alongside, the outside atmospheric pressure also decreases. Hence, the volume of the ballonets is adjusted to account for the change in outside pressure. Ballonets are automatically controlled by the flight control system to maintain a constant pressure differential by changing the ballonet volumes. This requires the pressure and altitude feedback into the control system.

A higher internal pressure will be maintained in severe weather conditions (rain, ice, thunderstorm) to increase tension of the envelop fabric and maintain hull shape. Also, as the airspeed of the airship increases, the internal pressure will be slightly increased to avoid the nose of the airship from denting inwards.

The ballonets are also used for static pitch and roll trim. The ballonet trim controllers are designed for both manual and automatic control. In the automatic mode, the ballonet trim chase the control surface deflection eventually releasing all the pressure of the control stick. To avoid the controller chase, the ballonet trims can be controlled manually using the trim wheels. The response times for the ballonets are generally slower than the fin response and therefore they are mainly used for sustained attitude requirements.

The sub-scale model does not have ballonets installed so this part of the control system is not activated.

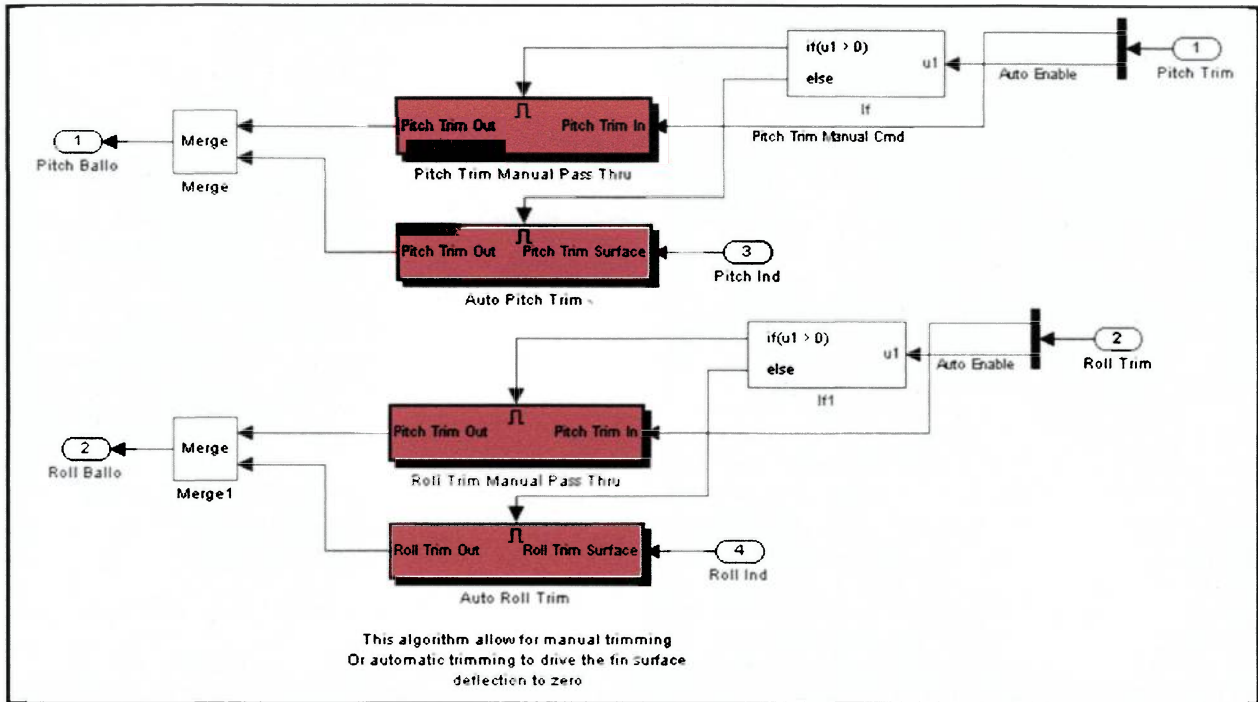


Figure 22: Ballonet Trim Controller Block

3.3 Graphical User Interface (GUI)

The graphical user interface has two main displays. Figure 23 shows the position, orientation, and the thrust of the four main engines. Figure 24 shows the attitude (roll and pitch) of the airship. These two displays are created in Simulink animation blockset.

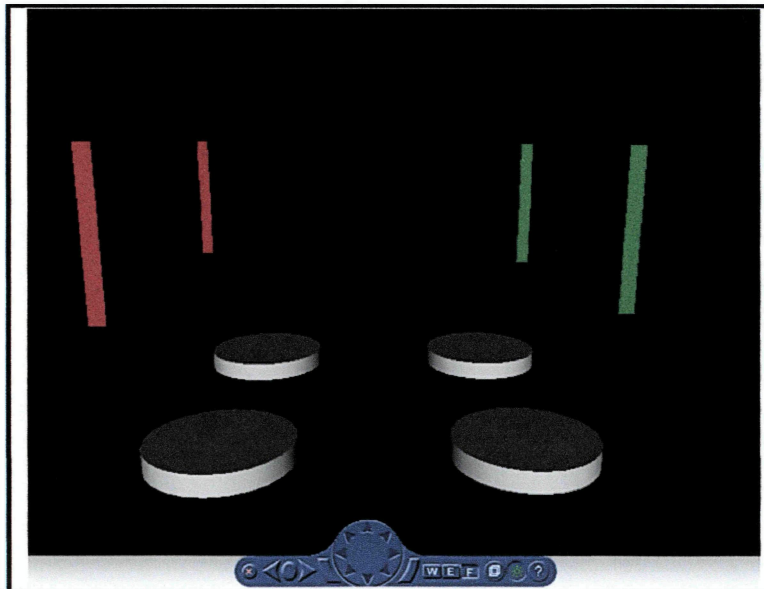


Figure 23: Engine Orientation and Throttle Display

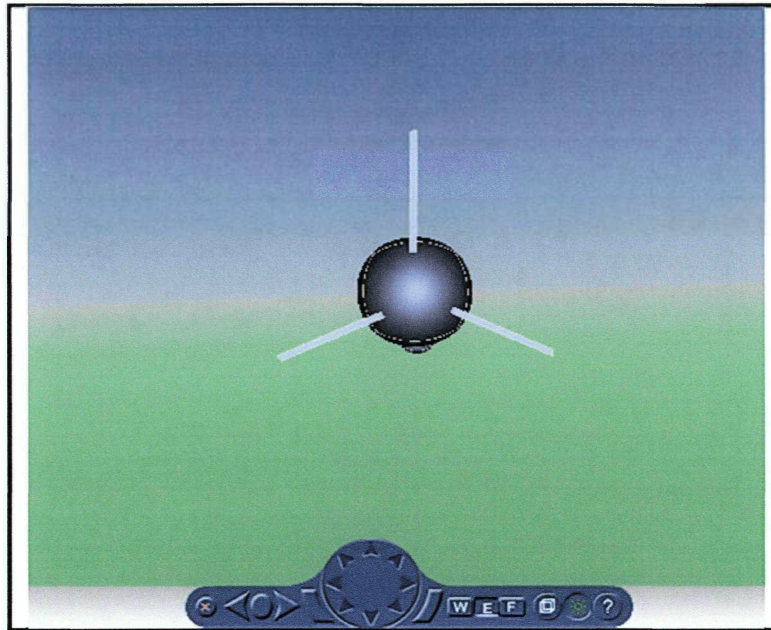


Figure 24: Airship Attitude Orientation

The third component of the display sub-system is the instrument cluster, as shown below. The instrument cluster contains objects such as digital roll, digital pitch, analog heading, bow, and tail motor thrusts.

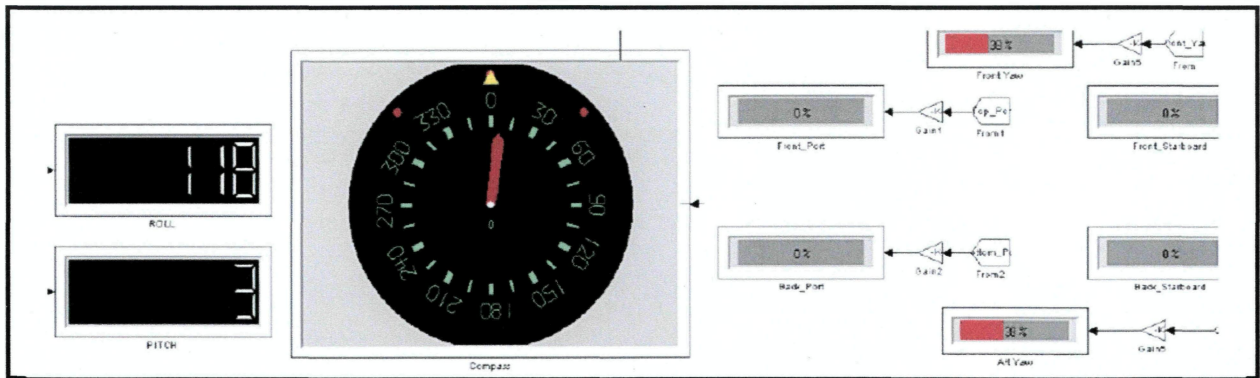


Figure 25: Instrument Cluster

These two virtual blocks combine with the instrument cluster forms the complete display system for the blimp as shown below:

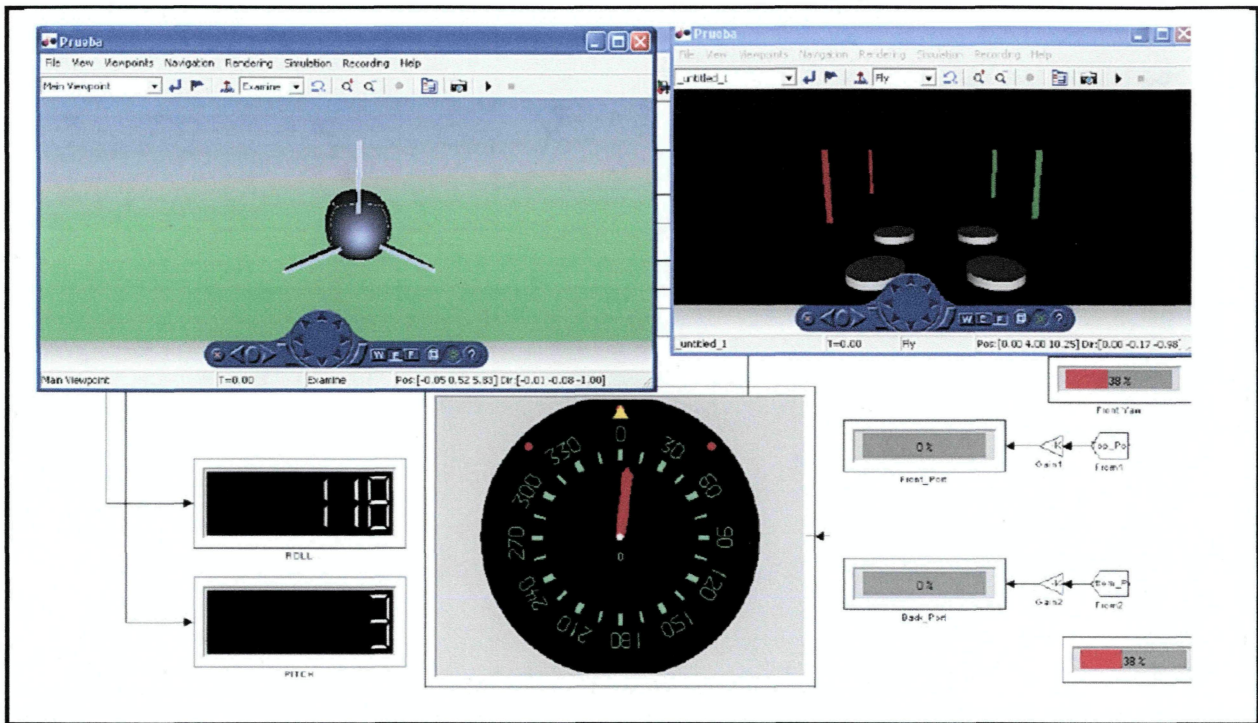


Figure 26: Airship Display System

3.4 Servo and Motor Command

The control vector is the main bus of the system. The control vector passes through all the control logic and carries the actuation commands for the servo and motors. The control vector components and description is shown in the following table:

Table 6: Servo and Motor Command

Component	Description
Fin_1	Angle for aerodynamic surface 1
Fin_2	Angle for aerodynamic surface 2
Fin_3	Angle for aerodynamic surface 3
Top_Port_Throttle	Thrust for front left engine vector
Top_Port_Vector	Three component angles that define the thrust line for the front left engine
Top_Starboard_Throttle	Thrust for front right engine vector
Top_Starboard_Vector	Three component angles that define the thrust line for the front right engine

Bottom_Port_Throttle	Thrust for aft left engine vector
Bottom_Port_Vector	Three component angles that define the thrust line for the aft left engine
Bottom_Starboard_Throttle	Thrust for aft right vector
Bottom_Starboard_Vector	Three component angles that define the thrust line for the aft right engine
Bow_Throttle	Thrust for bow engine
Bow_Vector	Three component angles that define the thrust line for the bow engine
Tail_Throttle	Thrust for tail engine
Tail_Vector	Three component angles that define the thrust line for the tail engine

This information is then converted into hex format and grouped in packets. These packets are then transmitted wirelessly to the airship. The following figure shows a glimpse of this implementation.

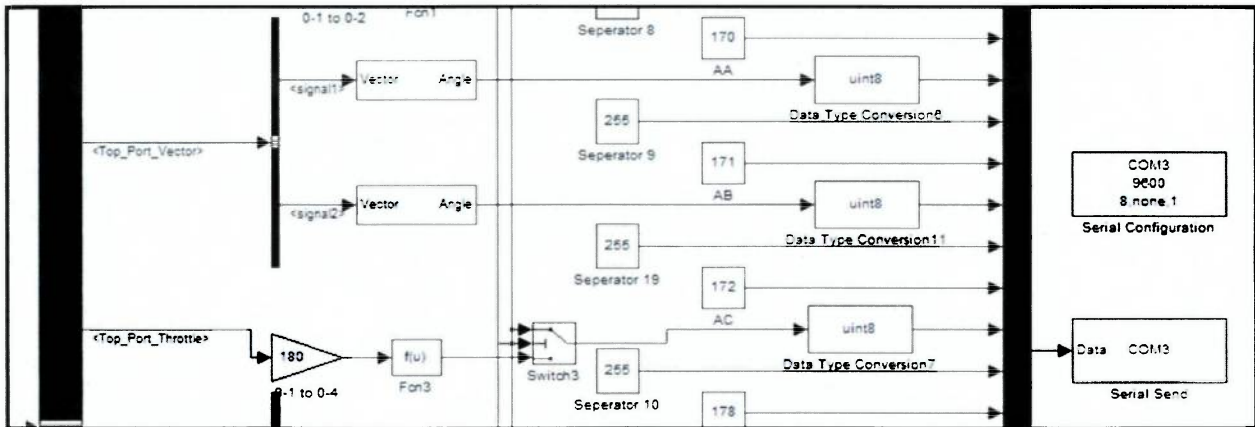


Figure 27: Command Packets

3.5 Joystick (User Input)

A Saitek Aviator joystick is used to provide user input into the system. The joystick is connected using a standard USB connection. Using the joystick block from the Aerosim Blockset library,

all signals are easily extracted to Simulink. These signals are then used generating control signals.

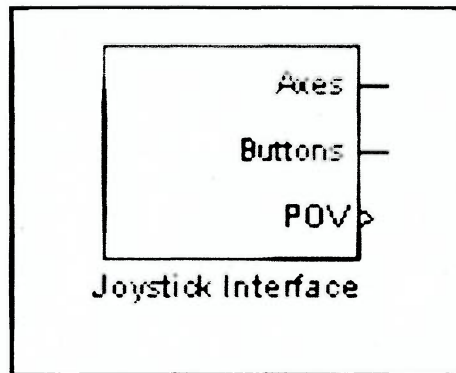


Figure 28: Joystick Interface

3.6 Navigation/Position Solution

The primary purpose of this sub-system is to calculate the 3D position of the airship inside the hangar. This sub-system also calculates the position error of the airship between the actual and the target position. The calculated position error then goes through a series of axis transformations to convert the data in terms of the airship body reference system.

The airship is flown in an indoor hangar environment, where a standard GPS device will have no range. To circumvent this problem, position through Stereo Vision is considered. For a stereo vision system, two cameras placed at a known location and orientations are used. These two cameras look at the same object in their individual camera reference frames. Triangulation in stereo vision is the task of computing the 3D position of points in the images, given the disparity map and the geometry of the stereo setting. To accurately compute the 3D position, the following process has been followed.

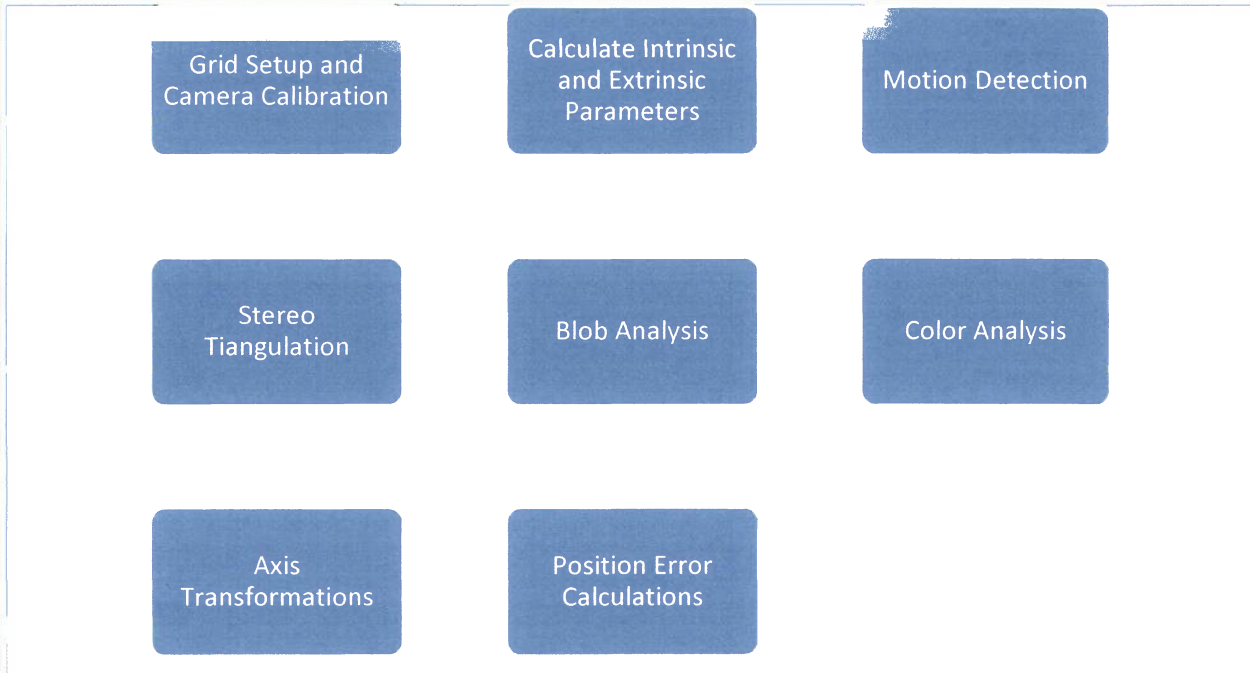


Figure 29: Position Solution Process

Each of these steps is discussed in the following sections.

3.6.1 Intrinsic and Extrinsic Parameters

Two Dynex™ 1.3MP Webcam are used as cameras connection to the ground station using high speed USB 2.0 connections as shown in figure below. Each webcam captures video at 640 X 480 resolutions.

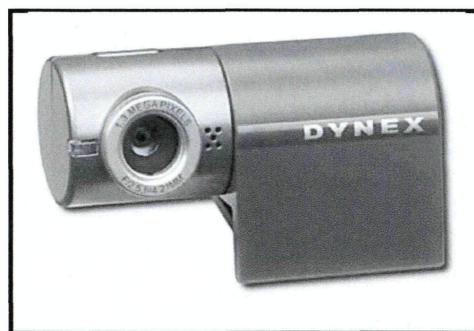


Figure 30: Dynex™ 1.3MP Webcam

Each camera has a set of internal and external parameters that need to be calculated for accurate triangulation.

The internal parameters are:

- 1) Focal length (fc): The focal length in pixels.
- 2) Principal point (cc): The principal point coordinates.
- 3) Skew coefficient (alpha_c): The skew coefficient defining the angle between the x and y pixel axes.
- 4) Distortions (kc): The image distortion coefficients (radial and tangential distortions).

These internal parameters are defined below:

Let **P** be a point in space of coordinate vector $\mathbf{X}\mathbf{X}_c = [\mathbf{X}_c; \mathbf{Y}_c; \mathbf{Z}_c]$ in the camera reference frame.

This point is now projected on the image reference frame. Let \mathbf{x}_n be the normalized (pinhole) image projection:

Equation 1

$$\mathbf{x}_n = \begin{bmatrix} \mathbf{X}_c/\mathbf{Z}_c \\ \mathbf{Y}_c/\mathbf{Z}_c \end{bmatrix} = \begin{bmatrix} x \\ y \end{bmatrix}$$

Let $r^2 = x^2 + y^2$.

After including lens distortion, the new normalized point coordinate \mathbf{x}_d is defined as follows:

Equation 2

$$\mathbf{x}_d = \begin{bmatrix} \mathbf{X}_d(1) \\ \mathbf{X}_d(2) \end{bmatrix} = (1 + \mathbf{Kc}(1)r^2 + \mathbf{Kc}(2)r^2 + \mathbf{Kc}(5)r^6)\mathbf{x}_n + \mathbf{dx}$$

Where \mathbf{dx} is the tangential distortion vector:

Equation 3

$$\mathbf{dx} = \begin{bmatrix} 2\mathbf{Kc}(3)xy + \mathbf{Kc}(4)(r^2 + 2x^2) \\ \mathbf{Kc}(3)(r^2 + 2y^2) + 2\mathbf{Kc}(4)xy \end{bmatrix}$$

The vector **kc** contains both radial and tangential distortion coefficients. Once distortion is applied, the final pixel coordinates $\mathbf{x}_{\text{pixel}} = [\mathbf{x}_p; \mathbf{y}_p]$ of the projection of **P** on the image plane is:

Equation 4

$$Xp = fc(1)(Xd(1) + \alpha_c * Xd(2)) + cc(1)$$

$$Yp = fc(2)Xd(2) + cc(2)$$

Therefore, the pixel coordinates vector x_{pixel} and the normalized coordinate vector x_d are related to each other through the linear equation:

Equation 5

$$\begin{bmatrix} Xp \\ Yp \\ 1 \end{bmatrix} = KK \begin{bmatrix} Xd(1) \\ Xd(2) \\ 1 \end{bmatrix}$$

Where KK is known as the camera matrix, and defined as follows:

Equation 6

$$KK = \begin{bmatrix} fc(1) & \alpha_c * fc(1) & cc(1) \\ 0 & fc(2) & cc(2) \\ 0 & 0 & 1 \end{bmatrix}$$

These parameters and their relative errors are calculated using a Camera Calibration Toolbox developed by Caltech.

The external parameters are:

- 1) Rotation Matrix
- 2) Translation Matrix

A 10 ft x 10 ft check board is laid on the floor which forms the basis of external parameter calibration. This check board is used as an intermediate reference frame between the camera reference frame and the body frame. The check board reference frame is shown in figure 31:

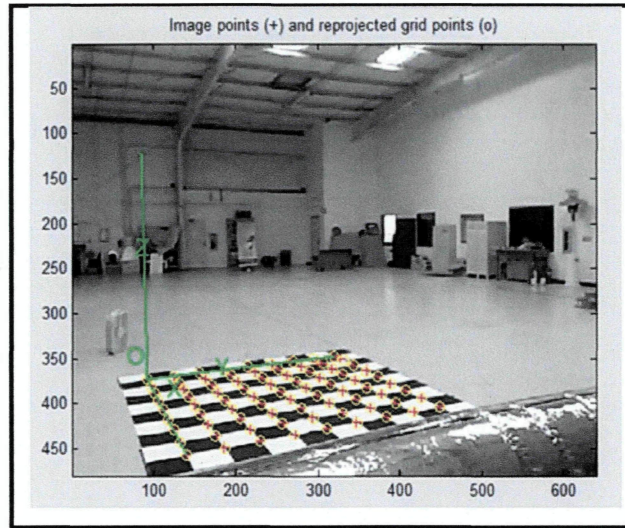


Figure 31: Check Board Reference Frame

The above figure shows the reference frame (O, X, Y, Z) attached to that calibration grid. Let P be a point space of coordinate vector $XX = [X; Y; Z]$ in the grid reference frame. Let $XXc = [Xc; Yc; Zc]$ be the coordinate vector of P in the camera reference frame. Then XX and XXc are related to each other through the following rigid motion equation:

Equation 7

$$XXc = Rc_1 * XX + Tc_1$$

In particular, the translation vector Tc_1 is the coordinate vector of the origin of the grid pattern (O) in the camera reference frame, and the third column of the matrix Rc_1 is the surface normal vector of the plane containing the planar grid in the camera reference frame. The same relation holds for the remaining extrinsic parameters. Once the coordinates of a point is expressed in the camera reference frame, it may be projected on the image plane using the intrinsic camera parameters.

Similarly to the intrinsic parameters, the uncertainties attached to the estimates of the extrinsic parameters are also computed by the toolbox.

3.6.2 Camera Calibration and Setup

Two cameras and a check board are used for stereo calibration. Both the left and right cameras have to be calibrated to calculate their internal and external parameters. The following process is similar for both cameras and only the process for the right camera is shown below. The first step in calibrating is to set the check board at a set location without moving it during the entire calibration process. Then multiple pictures of the check board from different orientations are taken. This stack of multiple pictures is shown below:

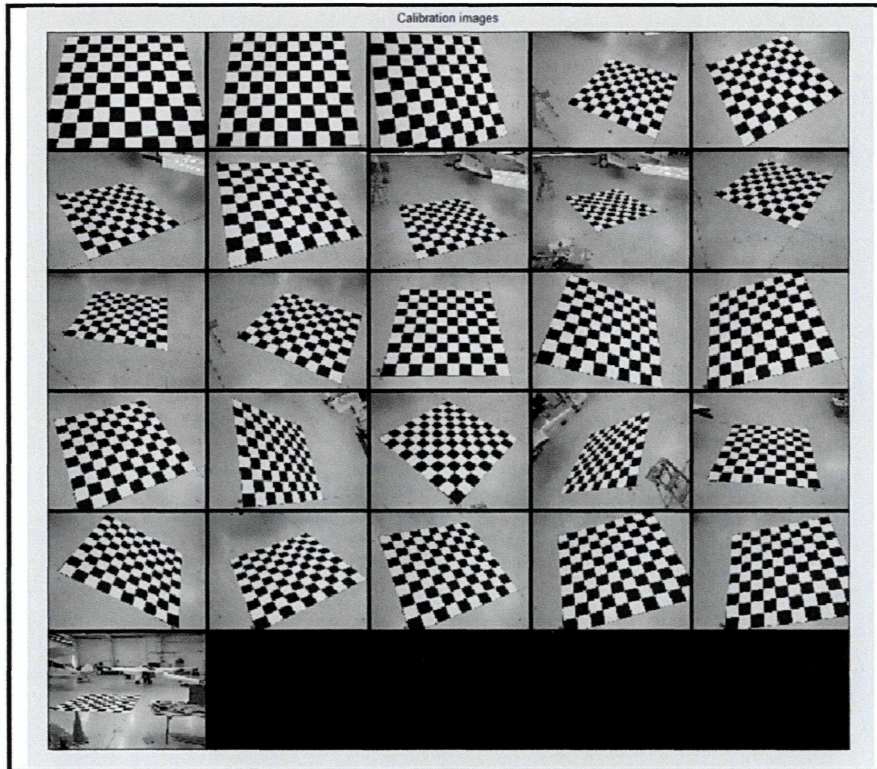


Figure 32: Uncalibrated Images

For each picture, the four corners have to be manually extracted as shown below:

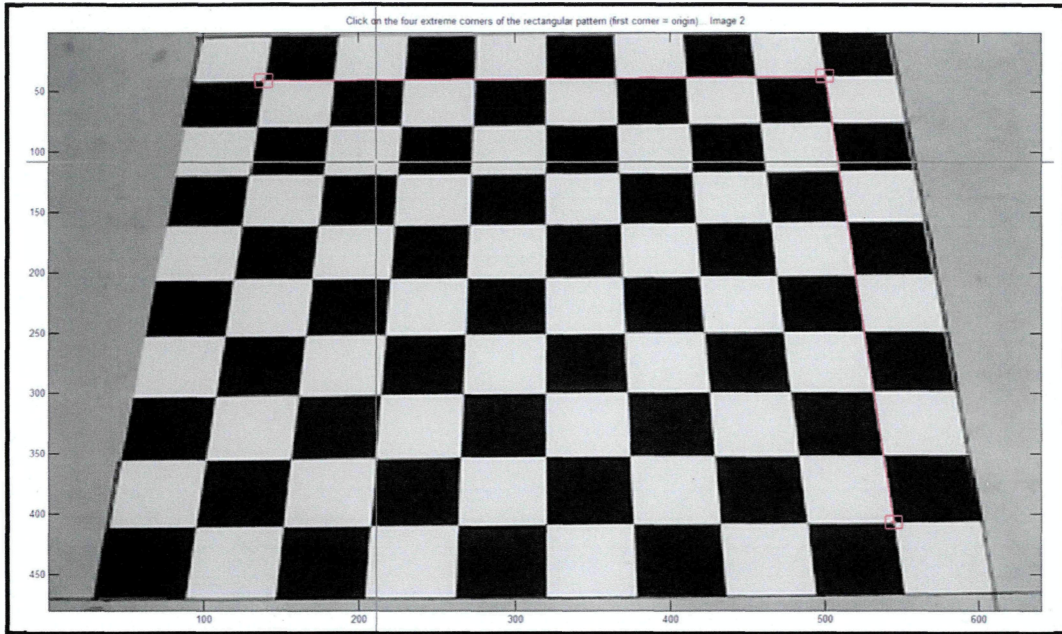


Figure 33: Manual Corner Extraction

The calibration toolbox extracts all the corners of the check board along with the X and Y axis in the check board reference frame. The origin in this reference frame is denoted by \mathbf{o} . The same steps are followed for all the images in the stack.

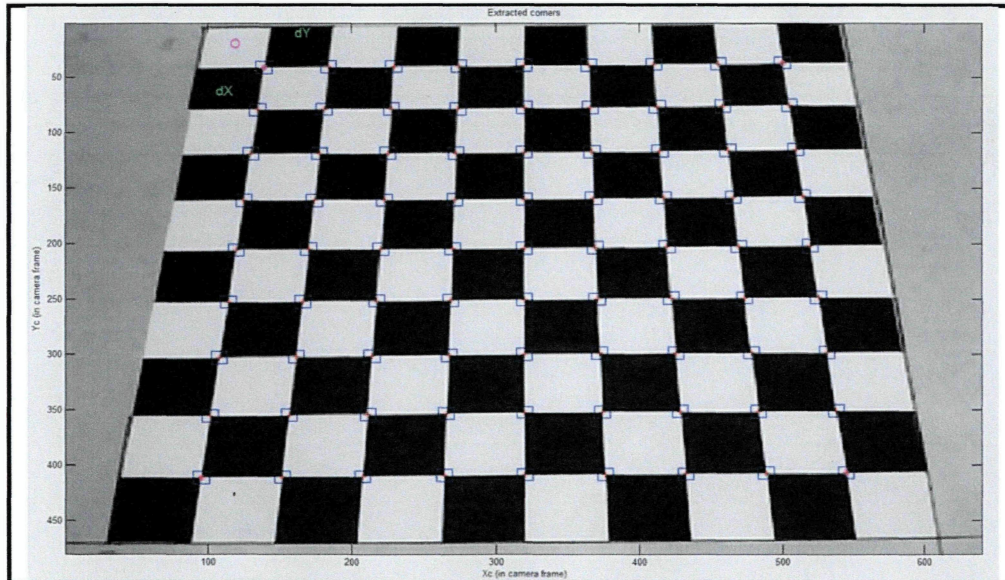


Figure 34: Extracting Grid Corners

The different orientations used for taking pictures of the grid are shown below along with the grid reference frame. This is known as the world-centered view. The same information is also shown in a camera-centered reference frame.

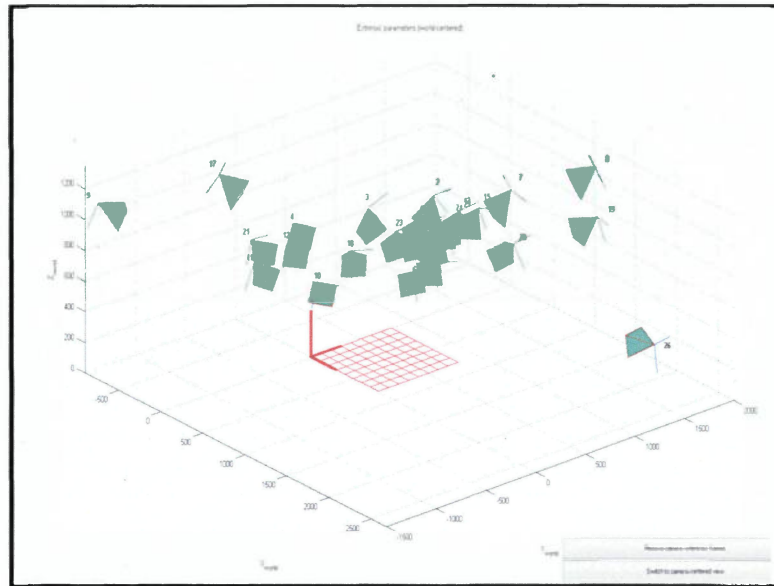


Figure 35: World Centered View

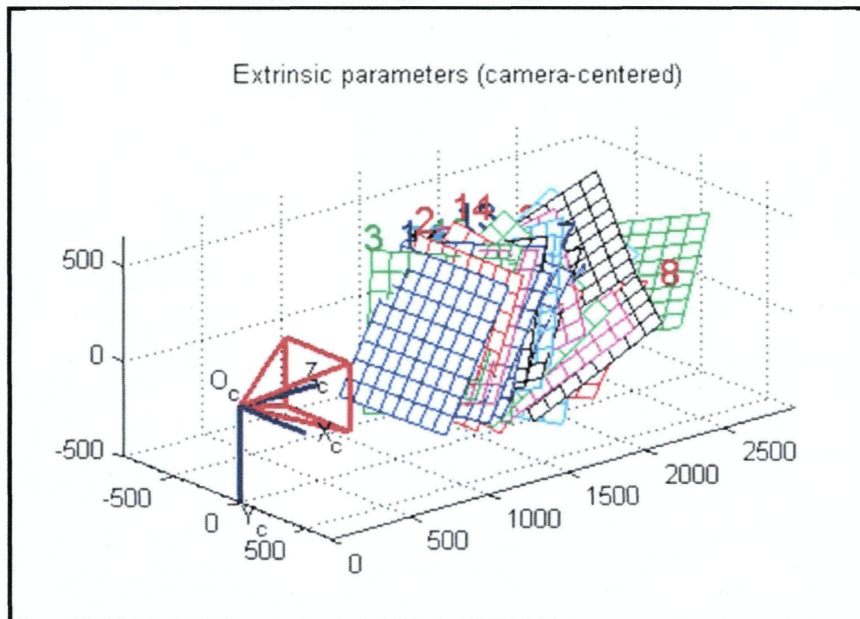


Figure 36: Camera-Centered View

The toolbox also calculates the error in extraction of all the corners. The point of the error analysis is to reduce the re-projection error in pixels. The initial error projection is shown in fig (a). Only one picture and set of corners shown by red plus signs has higher error in comparison. This picture was reprocessed to reduce the over projection error. The final result of this analysis is shown in right side of figure 37. The maximum projection error has reduced from 2 pixels to 0.5 pixels.

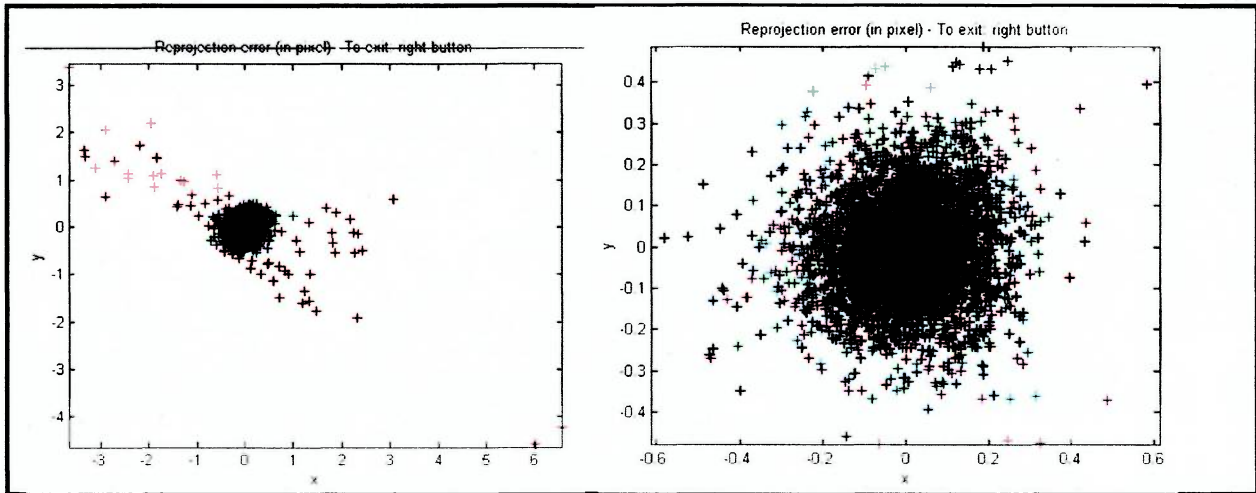


Figure 37: Pixel Projection Error

The next step is to select a proper distortion model for the camera. In order to make a decision on the appropriate distortion model to use, it is sometimes very useful to visualize the effect of distortions on the pixel image, and the importance of the radial component versus the tangential component of distortion. These distortion models are drawn using the calibration toolbox. These distortion models are shown below:

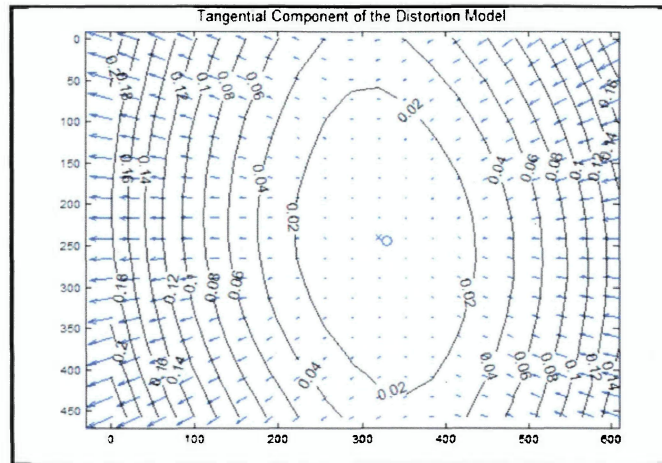


Figure 38: Tangential Distortion Model

There is no tangential distortion visible in the center of the image. The tangential distortion increases towards the camera corner. The radial component of distortion is also negligible at the center and increases towards the corner.

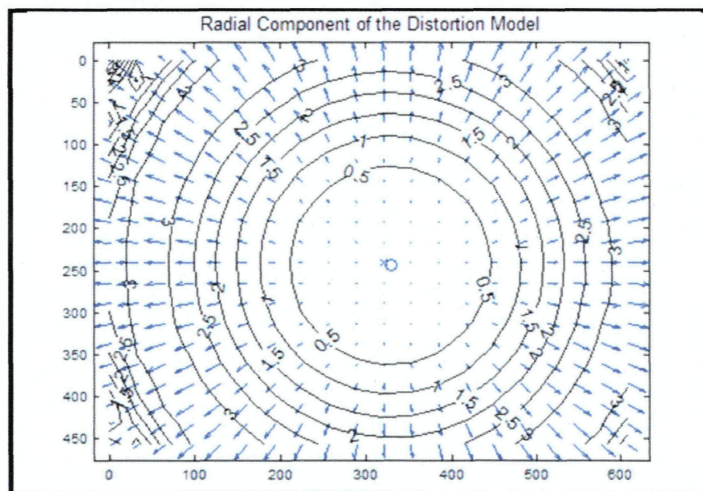


Figure 39: Radial Distortion Model

In comparing the magnitude of distortion, the tangential distortion is small compared to the radial distortion of the image. When both the distortions are added together, the tangential distortion is hardly visible. By inspection, only the radial distortion causes a significant effect, and is thus used for distortion correction.

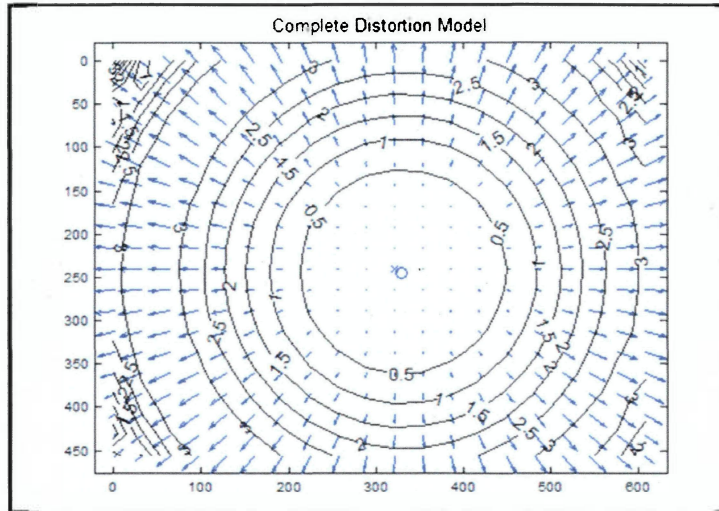


Figure 40: Complete Distortion Model

This distortion matrix is stored and used during stereo triangulation.

3.6.3 Solving the Correspondence Problem

One of the key problems with stereo triangulation is solving the “Correspondence Problem.” Finding paired of matched points such that each point in the pair is the projection of the same 3D point. Triangulation depends crucially on the solution of the correspondence problem. Ambiguous correspondence between points in the two images may lead to several different consistent interpretations of the scene. Hence, to reduce this problem, a target red light is installed on the airship. This target light can then be tracked by both the cameras and a set of vision filters can be used to isolate this target in both the camera frame. These vision filters (motion detection, color analysis) will be discussed in the following sections. This help solves the correspondence problem. To be able to see this target from all directions, a set of reference LEDs are used oriented in eight different directions. This target is shown in the figure below:

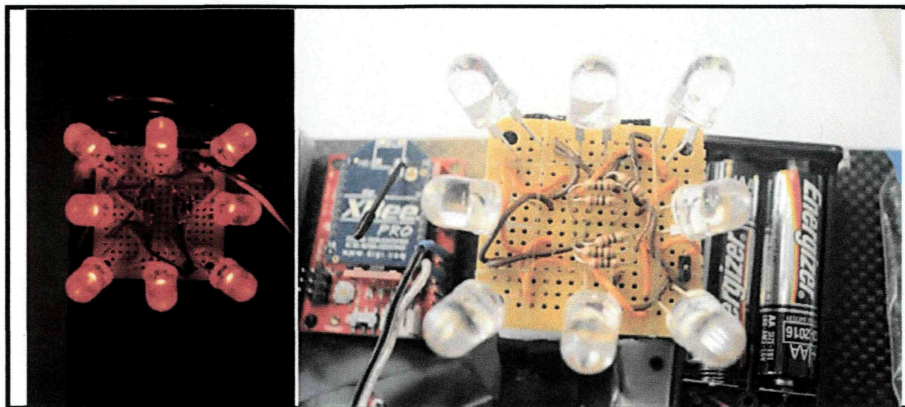


Figure 41: Onboard LED Target

The following figure shows the circuit diagram for the LED target setup.

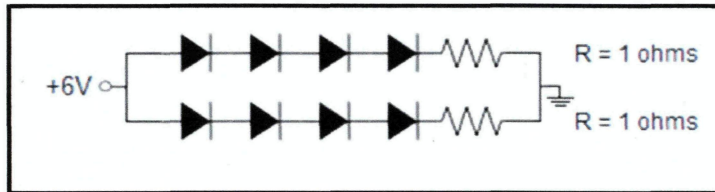


Figure 42: LED Circuit

3.6.4 Vision Filters

Three filtering techniques are used to help solve the correspondence problem.

- 1) Motion Detection – Isolate only moving objects
- 2) Color Analysis – Isolate red color.
- 3) Blob Analysis – Estimate target coordinates (X1, Y1) and (X2, Y2) in individual camera reference frames.

3.6.4.1 Motion Detection

The purpose of this filter is to isolate all the moving objects in the camera's view. This allows us to remove all the static noise in the background. This process gets rid of approximately 70-80% of the noise from the camera's view. This is the first filter that is applied to the raw video data. This raw video data is dissected into its primary color channels (Red, Green, and Blue). Each of these signals is processed individually. The raw video capture block is shown below:

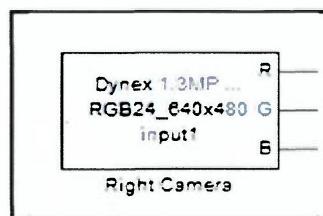


Figure 43: Right Camera Block

Each color signal then goes through a background estimator. The purpose of this block is to estimate the background in the camera view frame. Once the background is estimated, the

current video frame is then subtracted from the background. This mathematical operation subtracts the static background, and leaves the output with any object that is moving.

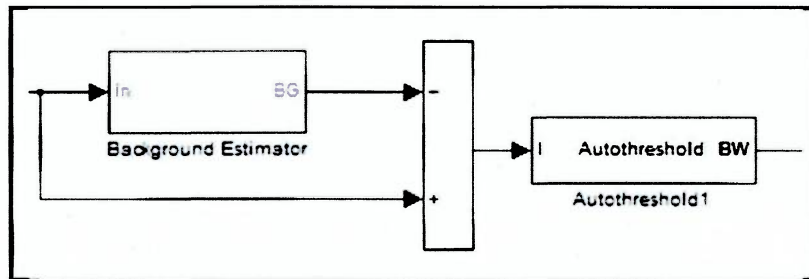


Figure 44: Background Estimation Filter

Three different background estimation methods are considered which have different benefits in different initial conditions. All three background estimators work on the same basic logic. Every video frame for each color signal is a 640 X 480 matrix. The estimator compares the value of each pixel to its previous value. Based on this difference, the logic for every estimation method is different. The temporal Median estimator method estimates the median of every pixel value over a fixed time. If this median value is within a predetermined range, the estimator then classifies that particular as either background object or moving object. If it is classified as a background object, the pixel value is set to zero (black). Objects that are identified as moving objects are set to the original pixel value. The output of all the estimation methods is a 3x640x480 matrix. The temporal median method doesn't have a predetermined range, and is calculated as an average value over the last 30 frames. Unlike the temporal median estimator method, where the background image once estimated remains the same for the duration of the flight, the temporal median method updates the background image periodically. The motion based background estimator method is a reversed estimated method. It tends to estimate already moving objects in the background during the estimation process and eliminates them. For example, if the background has a fluttering flag or a flickering light reflection, this method identifies such movement and identifies it as a static object. The implementation of these three methods is shown below:

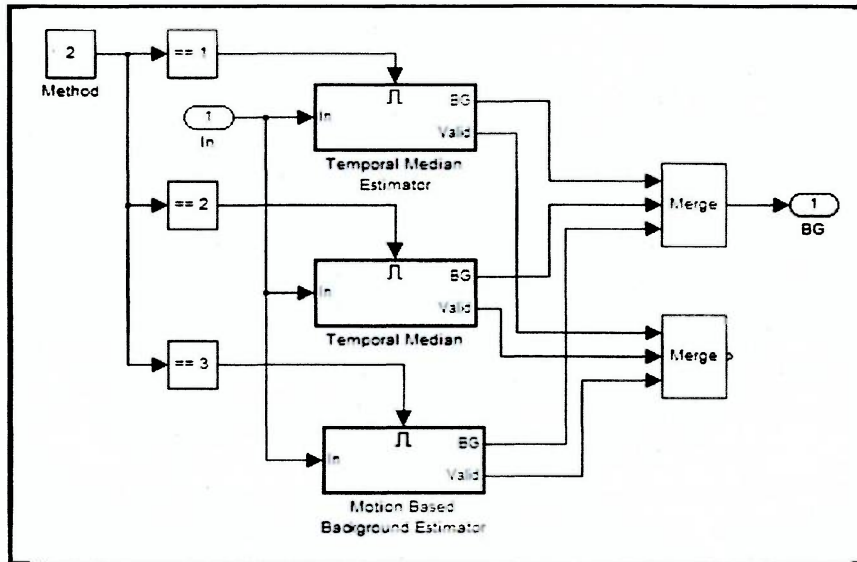


Figure 45: Background Estimators

3.6.4.2 Color Analysis

The three color signal outputs from background analysis are used as an input for color analysis. The objective of this analysis is to isolate any red objects and reject all other colors. To achieve this, a 640x480 green matrix is subtracted from the 640x480 red matrix. The blue 640x480 matrix is then subtracted from this result. This process removes all the traces of blue and green in the image. A surrounding factor was later added to correct for environment redness. This factor changes depending upon the sun, as the hangar where the airship was flown had open sky roofs.

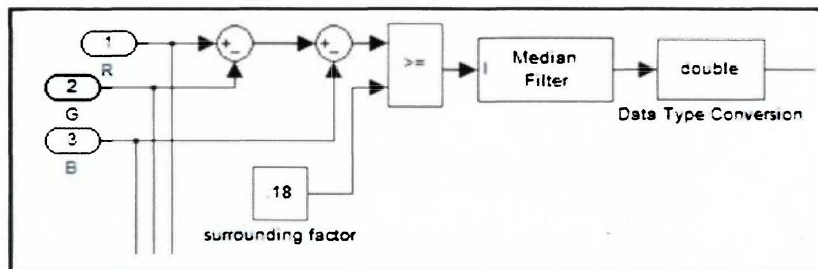


Figure 46: Color Analysis

This output then goes through a Median Filter and data conversion. The data conversion converts the red and black matrix into a black (0) and white (1) binary matrix.

3.6.4.3 Blob Analysis

The objective of the blob analysis is to calculate the centroid of the target. After applying motion detection and color analysis, the remaining objects in the video frame should only be the LED target light. The blob analysis then calculates the centroid of this target in terms of the pixel reference frame as shown below:

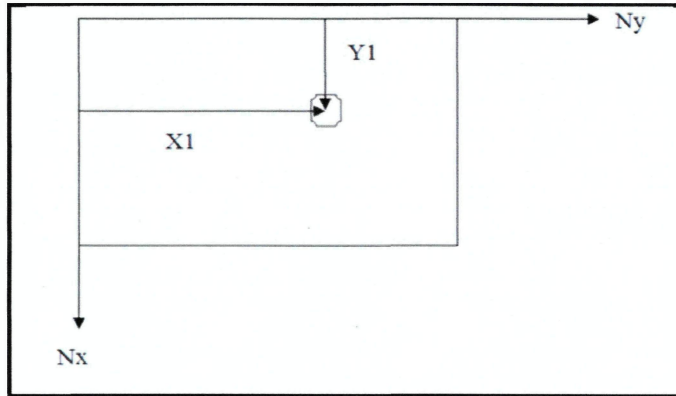


Figure 47: Pixel Reference System

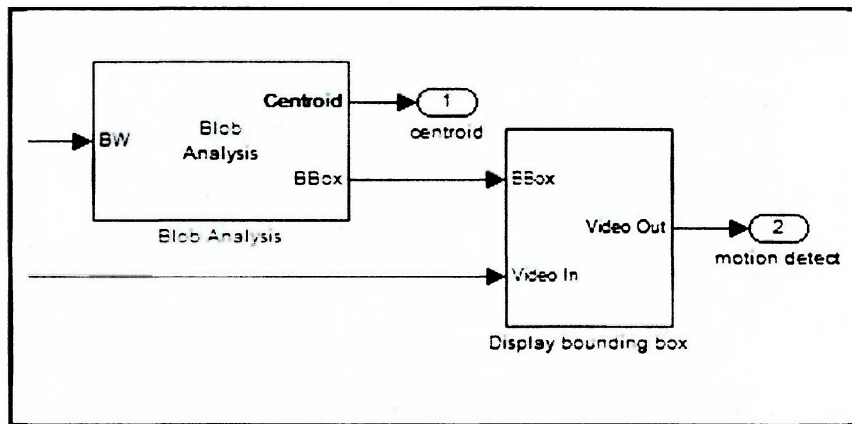


Figure 48: Blob Analysis

The centroid information is then used for stereo triangulation. To visualize this output, a bounding box is put around the target and superimposed on the raw video image. This information is calculated for both the cameras using the same process.

3.6.5 Stereo Triangulation

We now have all the information we need to triangulate the airship position. The stereo triangulation algorithm is coded using an embedded MATLAB function and is included in the appendix. The 3D position output of stereo triangulation is then sent to the ground control for position error calculation.

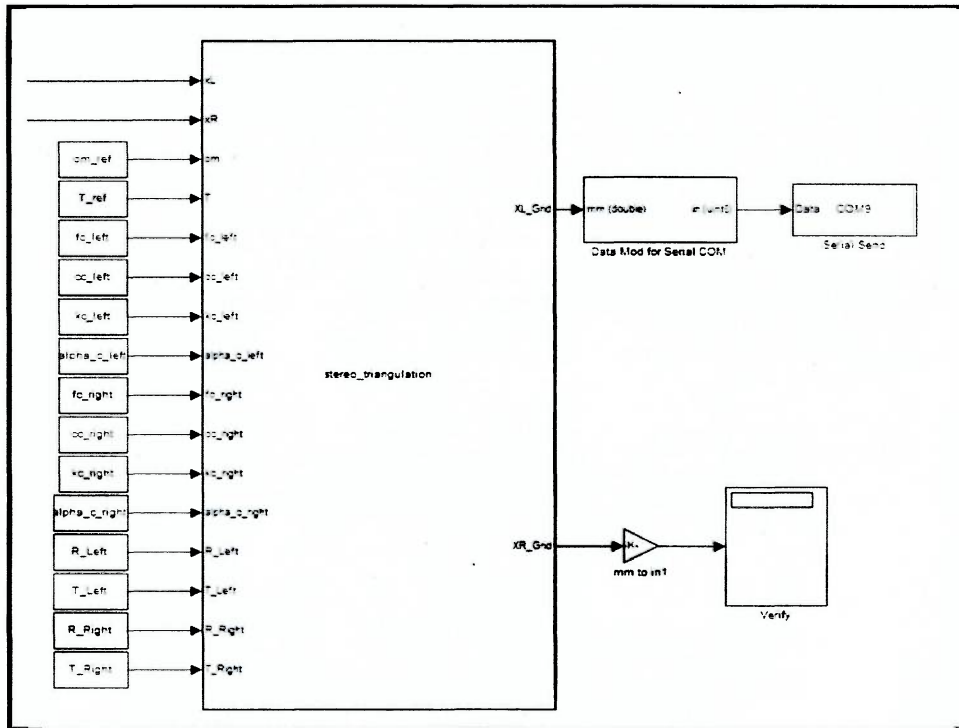


Figure 49: Stereo Triangulation

3.6.6 Axis Transformations

Many axis transformations take place during the entire position solution process which is shown below.

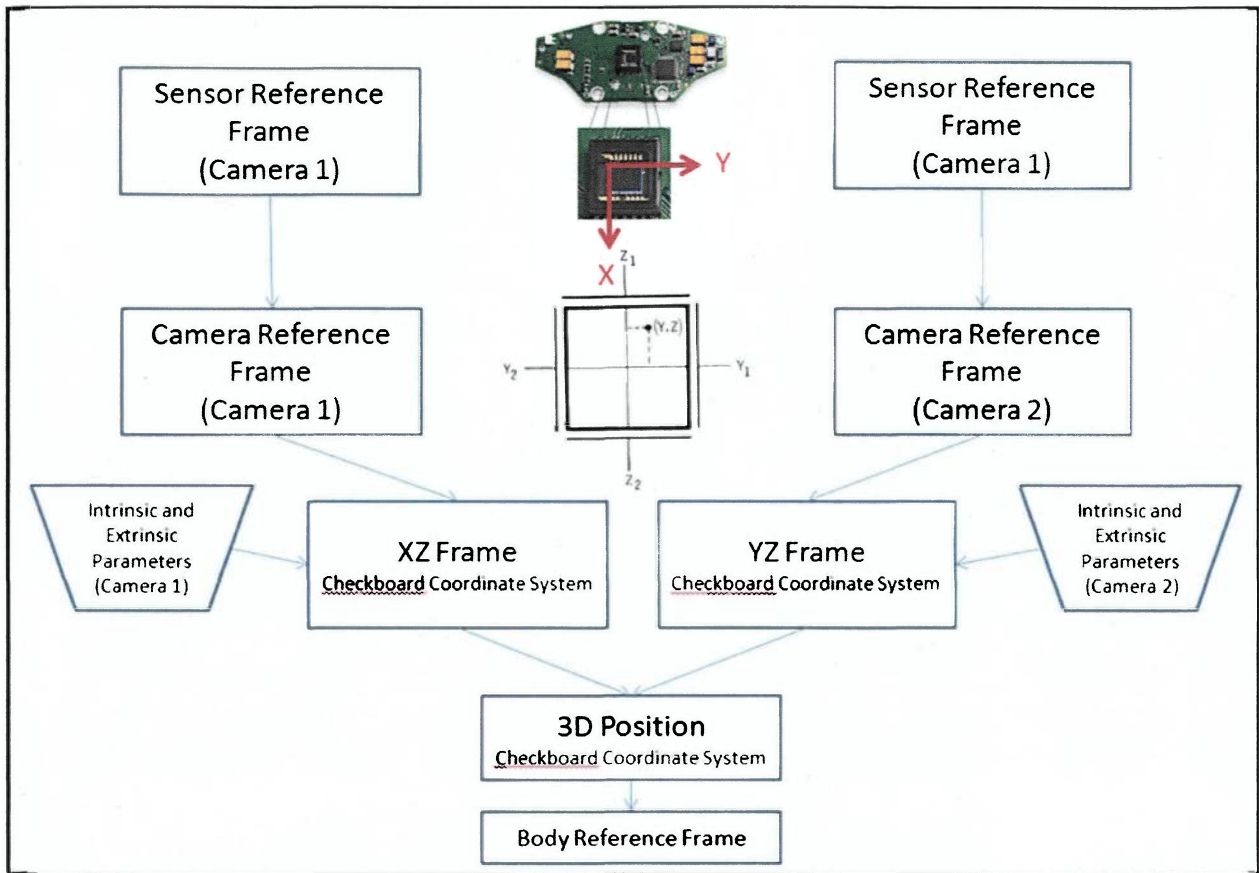


Figure 50: 3D Position Coordinate Transformations

The sensor reference frame (also known as a pixel reference frame) is first converted into Camera reference frame. The camera reference frame is the coordinate system adjusted from the top right corner to the center. Along with the intrinsic and extrinsic parameters, the object in the camera reference frame is converted into a 2D position in the check board reference frame (grid reference frame). Based on the 2D position from the left and right camera, the 3D position of the target is calculated in the check board reference frame. This information is then used to calculate the position error and converted into airship body reference frame. This process is discussed in the next section.

3.6.7 Position Error Calculations

The position error calculation is initiated using a user input joystick command. When position hold is initiated, the current position of the airship is stored. This information is used to calculate the position error for all the subsequent frames. The calculated position is in the check board

reference frame; hence, the position error calculated is also in the check board reference frame. The control system logic is designed assuming input is in the airship body reference frame. Hence, the position error in the check board reference frame is then converted into the body reference frame as shown below.

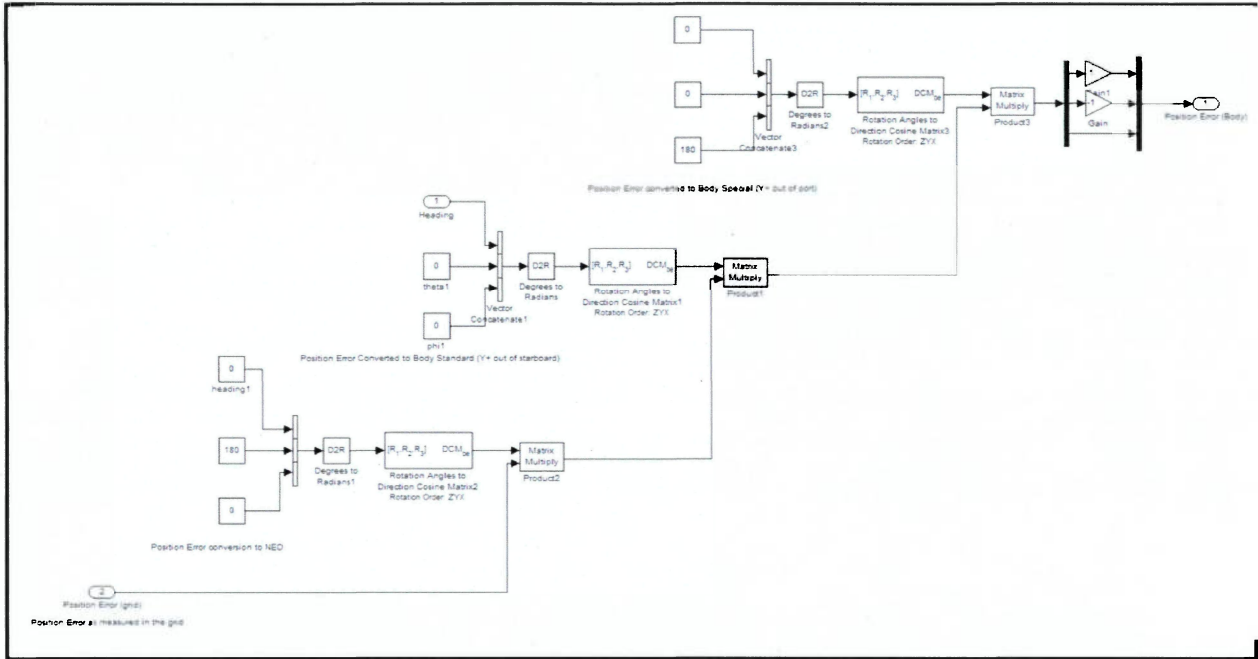


Figure 51: Position Error Coordinate Transformations

The final position error in the body reference system is then used as the feedback for the position hold control block.

3.7 Attitude Heading Reference System (AHRS) Solution

The AHRS subsystem block outputs the best reference solution for the airship. This data uses raw data from the Inertial Measuring Unit (IMU) and magnetometer. A Kalman filter is then implemented to reduce the error in signals. A very brief description of this system is given below.

3.7.1 Inertial Measuring Unit (IMU) and Magnetometer.

The IMU provides the following raw information:

- 1) Acceleration local X Axis
- 2) Acceleration local Y Axis
- 3) Acceleration local Z Axis
- 4) Angular rate local X Axis
- 5) Angular rate local Y Axis
- 6) Angular rate local Z Axis

The magnetometer provides the raw compass heading. The following picture shows the IMU used for this project.

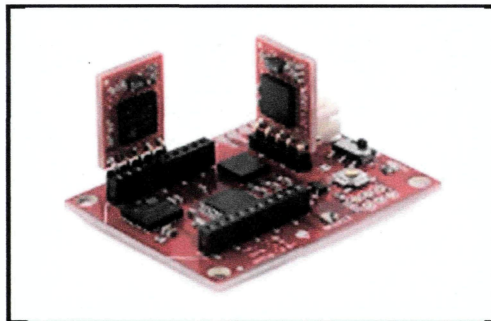


Figure 52: Spark Fun Atomic Magnetometer

3.7.2 Kalman Filter Implementation

The process used to generate a good reference solution is as follows:

- 1) Calculate Roll, Pitch, and Yaw angles using angular rates and kinematic equations.
- 2) Calculate Roll and Pitch using accelerations and gravity vector as reference.
- 3) Magnetic heading is used as a second source for yaw angle.

4) Apply a Kalman filter to these two sources of data to get the best possible result.

This implementation is shown in figure 53. Data from the IMU is captured and imported into Simulink using the S-function `serrea_sfun2` (included in Appendix). Similarly, data from the magnetometer is captured using S-function `read_sfunhead` (included in Appendix). The outputs of this implementation are Roll, Pitch, and Heading.

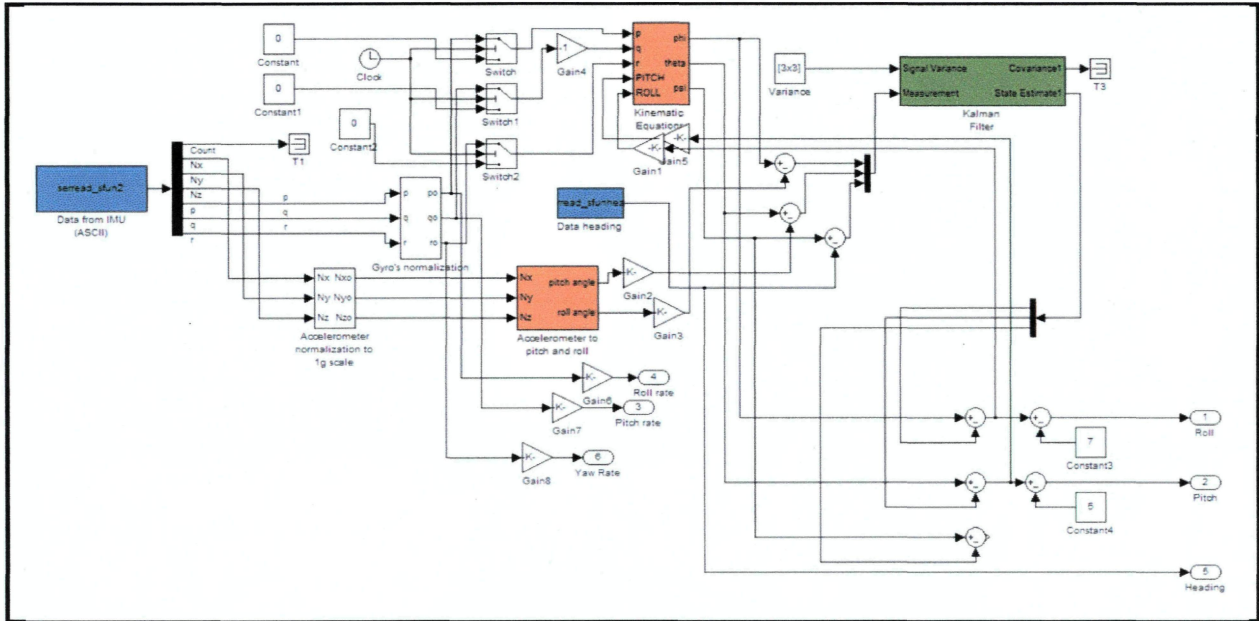


Figure 53: Kalman Filter

3.8 Communication and Actuation

Communicating control signals from the ground station to the airship is a very integral and complicated process, involving many different components. At the same time, airship attitude information is also communicated back to the ground station for feedback. The general data flow between the various components of the system is shown in the figure below:

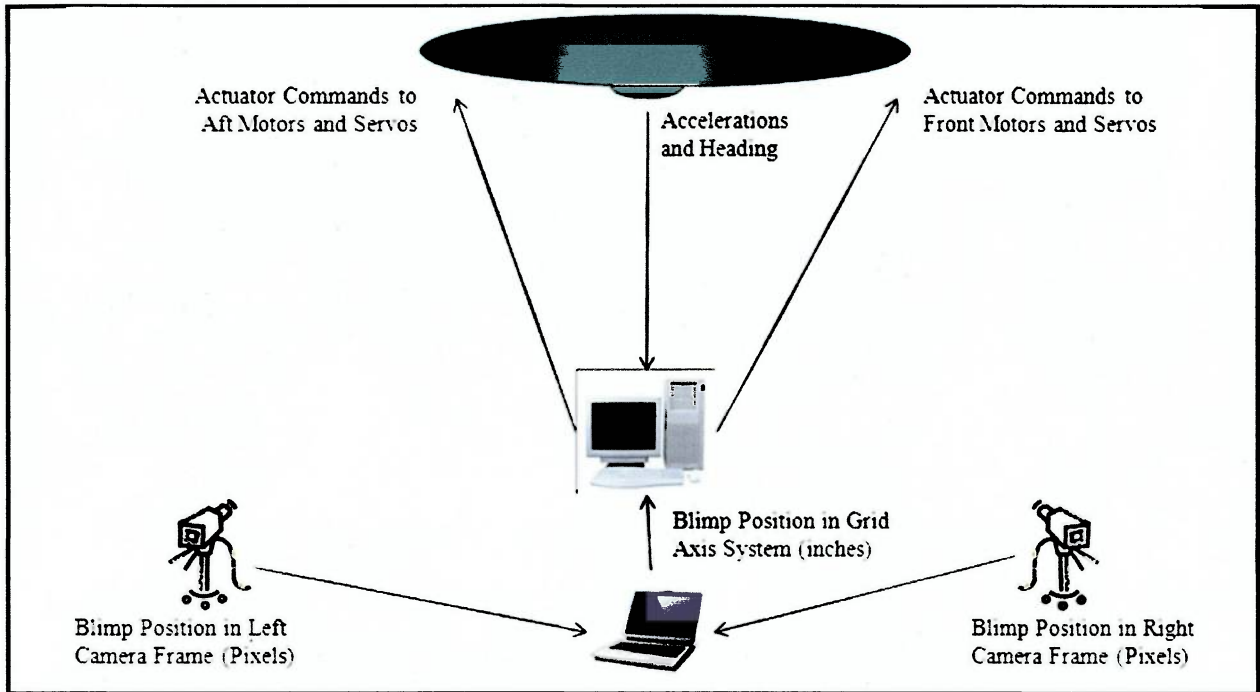


Figure 54: System Communication Overview

There are three main data flows for this system:

- 1) 3D Position data from laptop to the ground station (RS-232)
- 2) Accelerations and heading from AHRS system to the ground station (Wireless)
- 3) Actuator commands from ground station to the on-board controller (wireless)

To transmit any data, data is converted into appropriate packets. For wireless communication XBEEs are used which interface at 9600 bps. The technical information and communication protocol for Rs232 and wireless communication is beyond the scope of this thesis.

4. RESULTS AND ANALYSIS

This thesis provides proof of concept for the control design logic used to control a very large cargo airship. Various tests were conducted to test and analyze various systems of the airship and the different control laws implemented. These tests were performed and demonstrated in front of the thesis committee and the workings of the airship were video recorded. A brief description of the tests performed and the corresponding analysis is provided below:

4.1 Attitude Heading Reference System (AHRS) Results

To check the accuracy of the data calculated by the AHRS system, the IMU and the magnetometer were mounted on high precision digital inclinometer and measurements were taken every 5 degrees. An average of three sets of such readings was taken. Readings were taken separately along the roll and pitch axis. The following table provides the measured angles by the inclinometer and the AHRS system.

Table 7: AHRS Accuracy Results

Inclinometer (deg)	Average Roll (deg)	Average Pitch (Deg)
-60.0	-54.3	-49.8
-55.0	-49.9	-45.4
-50.0	-47.6	-43.1
-45.0	-43.2	-38.7
-40.0	-41.5	-37.0
-35.0	-36.3	-31.8
-30.0	-31.3	-26.8
-25.0	-24.5	-20.0
-20.0	-20.9	-16.4
-15.0	-14.6	-10.1
-10.0	-10.7	-6.2
-5.0	-4.8	-0.3
0.0	0.5	5.0
5.0	4.8	9.3
10.0	10.2	14.7

Inclinometer (deg)	Average Roll (deg)	Average Pitch (Deg)
15.0	16.7	21.2
20.0	19.8	24.3
25.0	24.7	29.2
30.0	28.9	33.4
35.0	33.7	38.2
40.0	39.4	43.9
45.0	43.6	48.1
50.0	47.2	51.7
55.0	50.2	54.7
60.0	56.7	61.2

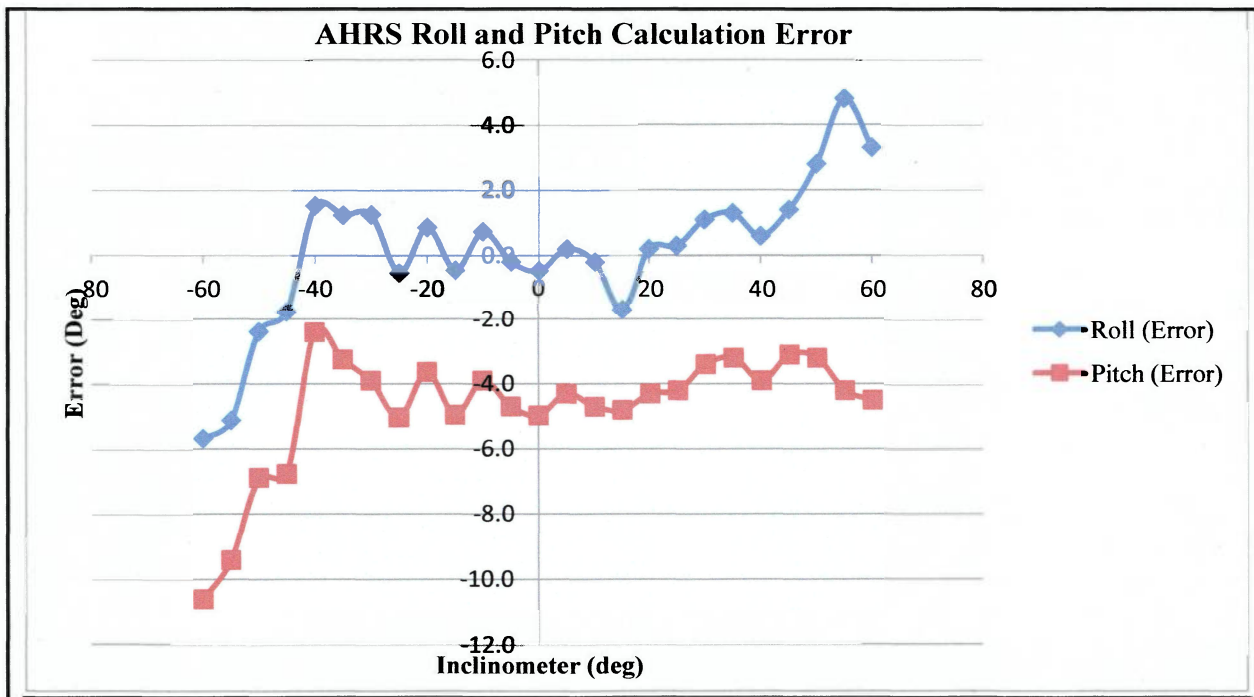


Figure 55: AHRS Results

The above graph shows the error in calculation of the roll and pitch angle using the AHRS system. For roll angle, the error in calculation is less than 2 degrees for angles up to 45 degrees. The error in calculation increases as the bank angle increases. There is an approximately 4.5 degrees of bias in the calculation of the pitch angle. This error is a result of

improper mounting of the IMU on the inclinometer. The IMU has various pins on the bottom, which restrict us from mounting it flat against the inclinometer surface. Thus, on the airship a bias parameter is included to level the static roll and pitch values. This bias value changes every flight based on the relative mounting of the IMU on the gondola.

Another important parameter under consideration is the update rate of the AHRS system. Proper tools were not available to test and measure this parameter, although general observations were made. The roll and pitch values update at a very slow rate. Although this was not considered an issue for our purpose, as the overall airship dynamic response is of very low frequency, and the slow update rate has never caused any lag induced control problems.

4.2 Vision Position System Results

The vision position system was tested for accuracy of 3D position solution compared to the actual measured position. Multiple points were randomly selected throughout the hangar and were measured from the origin of the grid reference frame system. The results of this are documented in the table below:

Table 8: Vision Position System Error

Xmeasured (ft)	Ymeasured (ft)	Xvision (ft)	Yvision (ft)	Xerror (ft)	Yerror (ft)
-10.000	-10.000	-10.331	-10.298	-0.331	-0.298
-5.000	-5.000	-4.987	-5.122	0.013	-0.122
0.000	0.000	0.013	0.022	0.013	0.022
5.000	5.000	5.214	5.102	0.214	0.102
10.000	10.000	10.320	10.420	0.320	0.420
15.000	15.000	15.750	15.970	0.750	0.970
20.000	15.000	21.200	15.460	1.200	0.460
25.000	15.000	28.478	15.840	3.478	0.840
30.000	15.000	33.456	15.760	3.456	0.760

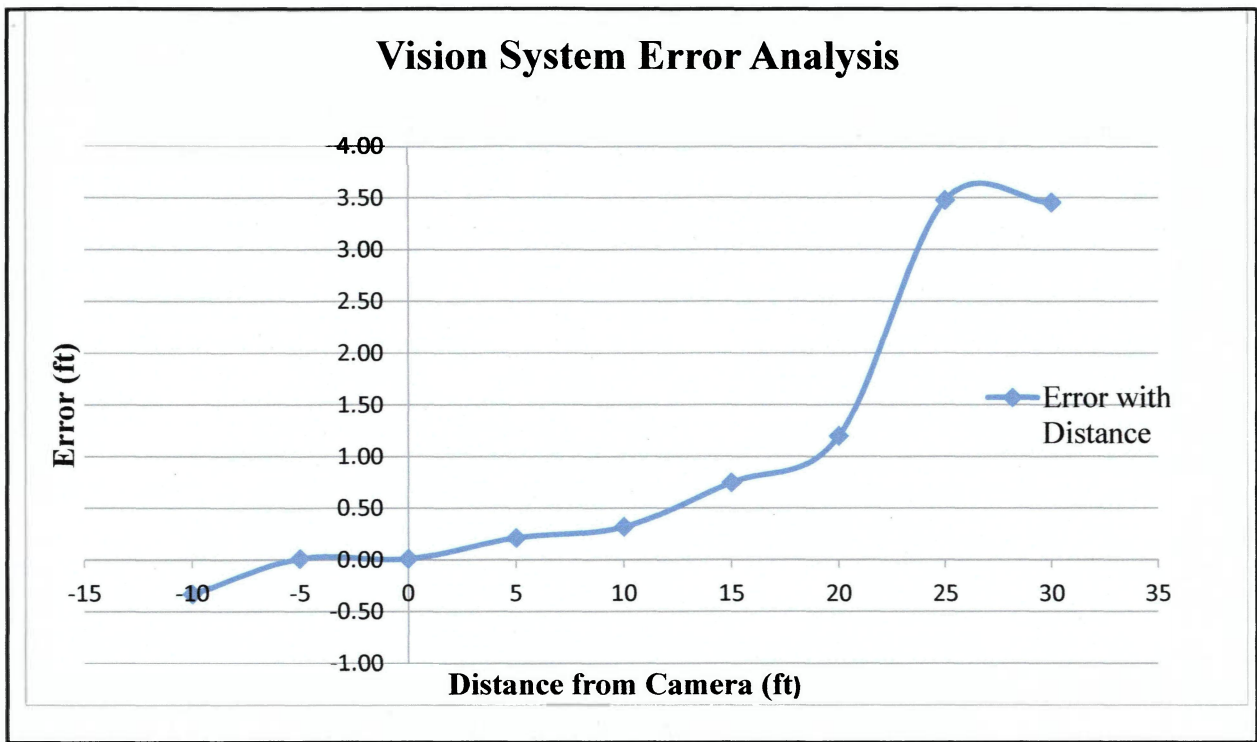


Figure 56: Vision System Error Analysis

From the graph it is clear that the error in position solution increases with distance from the cameras. The error is less than 1ft, up to a distance of 18.5ft from the camera position. The vision system was unable to track the LED lights placed 30ft away from the camera. Many reasons contribute to this error as discussed below:

- 1) Environmental Interference: Many filters are applied to the raw video signal to reduce atmospheric interference. Although as the distance between the camera and the LED source increases, the relative size and the intensity of the LED source reduces. Thus the environmental interference has a bigger influence as distance increases.

- 2) Correspondence Problem: On rare occasions, the left and right camera may track different objects at a given instance, hence resulting in an incorrect calculation of 3D position.

4.3 Control System Results

The various control logic implemented were tested in a series of flight tests. Although, due to the nature of these tests, there are no numerical results calculated. Roll hold and Pitch hold work very effectively. The airship has a natural tendency to level, which assists the dynamic stability system. The Low Speed Mode and High Speed Mode of the airship are effective in their individual operational envelop. In low speed mode, the control logic allowed the airship to successfully translate in all four directions. The high speed mode was effective in maneuvering the airship around the hangar. The heading hold system maintained the airships heading within 10 degrees, when activated.

One of the main research topics of this thesis was to study the effectiveness of the control system under crosswind conditions. To test this, the airship was commanded to hold a given position and heading. Manual fans were used to blow the airship away from its center. It was observed that the airship had a tendency to maintain its position in low winds condition. When the airship was displaced from its targeted hold position, the airship tends to return back to its original position. Although in most instances the airship overshoot the target position. Gains were further adjusted to resolve this issue, which minimized this effect.

One major reason for the poor performance of the position hold system is the accuracy of the thrust vectoring and power output. The control assumes the engines can be rotated exactly without any actuator errors and the thrust rating is accurate. So when the control system may command a particular servo to turn 45 degrees, the actual rotation of the servo can vary between ± 3 degrees. Similarly, due to the low fidelity of the speed controllers, a thrust of the engines is accurate to within $\pm 15\%$. The control system also assumes that there is no warping of the structure. Also the servos and engines are all mounted along the established thrust line. In reality, the particular aspect ratio of the airship and the structural design, leads to warping of the sub-scale model. As a result the thrust line for engines is different resulting in unbalanced thrust vectoring.

A few pictures from the test flights of the sub-scale model are shown below:



Figure 57: Airship in Flight # 1

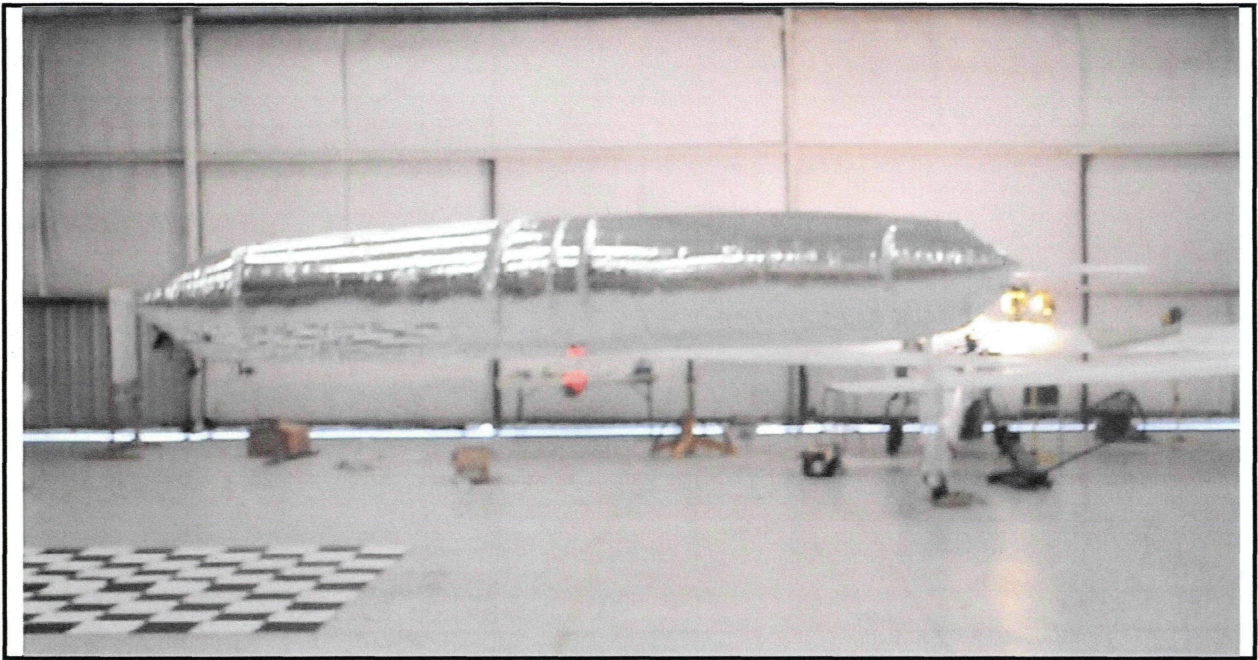


Figure 58: Airship in Flight # 2

5. CONCLUSION AND RECOMMENDATIONS

The airship was successfully flown in the hangar and the implemented control laws were tested. The roll and pitch stabilization controller are very effective, as they are assisted by the static tendency of the airship to stabilize itself. The stereo-vision system serves the purpose of providing a position solution in the absence of a GPS signal. The position hold system tends to bring the airship towards the target position, although the gains need to be improved to reduce overshoot. The airship control laws maintain airships position and direction in low wind conditions.

5.1 Future Work

A vast amount of research was done on this airship. Many different methods were used to achieve the target and successfully fly the airship. Many improvements can be made to the system, as listed below:

1. Use of three cameras and stereo triangulation methods to estimate position and attitude of the airship. A three LED target system can be used to achieve this.
2. Add aerodynamic control surfaces to directly test these effects in low and high wind conditions.
3. Add ballonets to the airship to test the ballonet control system.
4. Improve position hold gains to get better control solution.
5. Altitude hold can be implemented which will further assist cargo operations.

6. REFERENCES

- ¹ Nicolai, Leland M. Fundamentals of aircraft and airship design. Reston, VA: American Institute and Aeronautics and Astronautics, Inc., 2010
- ² Khoury, G.A. Airship Technology. Cambridge, NY: Cambridge University Press, 2004
- ³ Shock, James and Smith, David. The goodyear Airships. Bloomington, IL: Airship International Press, 2002
- ⁴ Bouguet, Jean-Yves. Camera Calibration Toolbox. Pasadena, CA.
<http://www.vision.caltech.edu/bouguetj/calib_doc/>
- ⁵ Roal, Jitendra R. Flight Mechanics Modeling and Analysis. Boca Raton, FL: CRC Press, 2009.
- ⁶ Siegwart, Roland. Introduction to Autonomous Mobile Robots. Cambridge, MA: The MIT Press, 2007
- ⁷ Arduino. 2010. <www.arduino.cc>
- ⁸ XBEE. 2011. Digi International Inc. <www.digi.com>
- ⁹ Sparkfun. 2010. Sparkfun Electronics. <www.sparkfun.com>

7. APPENDIX A: Printed Circuit Board (PCB) Design

To reduce the complexity of wiring between components, a PCB was designed and manufactured. This PCB was used to mount the XBEE, ARDUINO and other hardware connections directly onto it, thus reducing wiring weight and complexity. The PCB design is shown in the figure below:

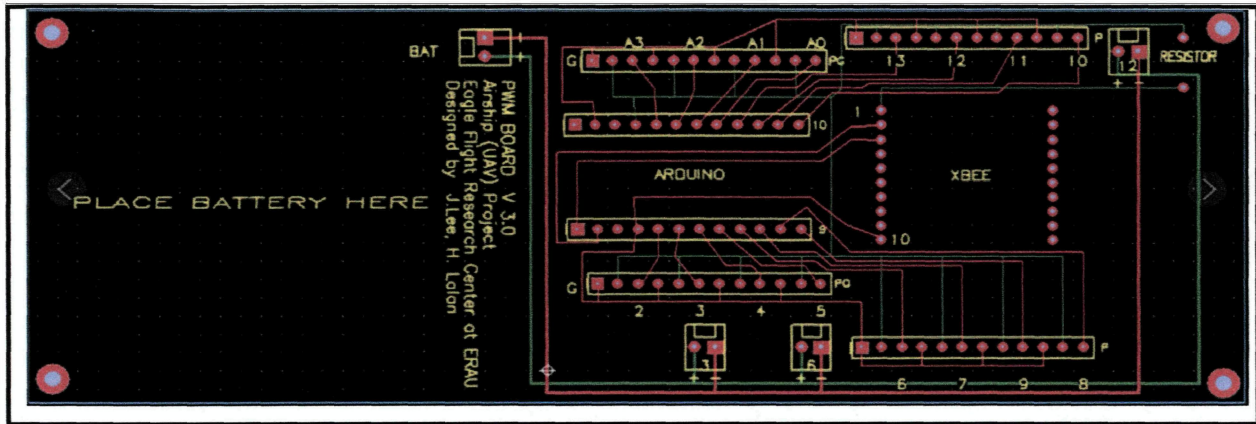


Figure 59: PCB Design